Fire, vegetation and Holocene climate in a south-eastern Tibetan lake: a multi-biomarker reconstruction from Paru Co

Alice Callegaro[1,2], Dario Battistel[1], Natalie M. Kehrwald[3], Felipe Matsubara Pereira[1], Torben Kirchgeorg[1], Maria del Carmen Villoslada Hidalgo[1], Broxton W. Bird[4], and Carlo Barbante[1,2]

[1]Dipartimento di Scienze Ambientali, Informatica e Statistica, Università Ca' Foscari Venezia, Venezia, 30172, Italia
[2]Istituto per la Dinamica dei Processi Ambientali-CNR, Venezia, 30172, Italia
[3]Geosciences and Environmental Climate Change Science Center, U.S. Geological Survey, Denver Federal Center, Denver, CO 80225, USA
[4]Department of Earth Sciences, Indiana University–Purdue University, Indianapolis, IN 46208, USA

Correspondence to: Alice Callegaro (alice.callegaro@unive.it) and Natalie M. Kehrwald (nkehrwald@usgs.gov)

Abstract. The fire history of the Tibetan Plateau over centennial to millennial timescales is not well known. Recent ice core studies reconstruct fire history over the past few decades but do not extend through the Holocene. Lacustrine sedimentary cores, however, can provide continuous records of local environmental change on millennial scales during the Holocene through the accumulation and preservation of specific organic molecular biomarkers. To reconstruct Holocene fire events and vegetation changes occurring on the south-eastern Tibetan Plateau and the surrounding areas, we used a multi-proxy approach, investigating multiple biomarkers preserved in core sediment samples retrieved from Paru Co, a small lake located in the Nyainqentanglha Mountains (29°47'45.6" N; 92°21'07.2" E; 4845 m a.s.l.). Biomarkers include *n*-alkanes as indicators of vegetation, polycyclic aromatic hydrocarbons (PAHs) as combustion proxies, fecal sterols and stanols (FeSts) as indicators of the presence of humans or grazing animals and finally monosaccharide anhydrides (MAs) as specific markers of vegetation burning processes. Insolation changes and the associated influence on the Indian Summer Monsoon (ISM) affect the vegetation distribution and fire types recorded in Paru Co throughout the Holocene. Early Holocene (10.7 – 7.5 cal ky BP) n-alkane ratios demonstrate oscillations between grass and conifer communities, resulting in respective smouldering fires represented by levoglucosan peaks, and high temperature fires represented by high-molecular weight PAHs. Forest cover increases with a strengthened ISM, where coincident high L/M ratios are consistent with conifer burning. The decrease in the ISM at 4.2 cal ky BP corresponds with the expansion of regional civilizations, although the lack of human FeSts above the method detection limits excludes local anthropogenic influence on fire and vegetation changes. The late Holocene is characterized by a relatively shallow lake surrounded by grassland, where all biomarkers other than PAHs display only minor variations. The sum of PAHs steadily increases throughout the late Holocene, suggesting a net increase in local to regional combustion that is separate from vegetation and climate change.

1 Introduction

The combustion of terrestrial vegetation by natural processes and anthropogenic activities are the primary sources of biomass burning (Simoneit et al., 1999). Humans add to the global burden of greenhouse gases (Bowman et al., 2009) through fire-related forest clearance. The impacts of greenhouse gases and associated global climate change on the frequency, intensity, duration, and location of biomass burning are not well understood and the contribution of fire emissions to past and future atmospheric composition are also unclear (IPCC, 2014). However, a recent study found that the synthesized Holocene fire record in eastern monsoonal China strictly tracks global atmospheric CO_2 concentration from Antarctica (Xue et al., 2018), but it is still not clear if fire and CO_2 triggered the rise in the other component or vice versa. Therefore, more studies are needed to investigate interactions with weather, climate, and landscape dynamics over a range of spatiotemporal scales.

Lake sediments archive high-resolution histories of sediment flux, as well as climatic, hydrological and ecological changes, for as long as the lakes preserve sediments through time (Yan and Wünnemann, 2014). Numerous recent studies demonstrate climatic variations throughout China and surrounding areas during the Holocene using lacustrine sedimentary records (Bird et al., 2017; Dietze et al., 2013; Liu et al., 2009; Opitz et al., 2012; Saini et al., 2017; Yanhong et al., 2006). The paleoclimate proxies used in these studies including carbonate percentages, mineralogy, grain-size distribution, elemental geochemistry, stable isotope composition, leaf wax long-chain *n*-alkanes, aquatic diatoms and terrestrial pollen, collectively record changes in hydroclimate and other environmental processes such as vegetation growth, detrital influx, volcanic eruptions. Within the Tibetan Plateau (TP), only a few studies examine past biomass burning by using charcoal (Herrmann et al., 2010; Miao et al., 2017) or black carbon. Polycyclic aromatic hydrocarbons (PAHs) are reported in the lake sediments from the TP spanning the last 2 centuries (Yang et al., 2016). Monosaccharide anhydrides (MAs), ammonia and black carbon in ice cores have been used as combustion proxies and indicators of fire on or influencing the Tibetan Plateau, but these records mainly cover the last century (Kaspari et al., 2011; Ming et al., 2008; Shugui et al., 2003; Xu et al., 2009; You et al., 2016b). To the best of our knowledge, no studies examine PAHs or MAs in sediments from the TP during the entire Holocene.

A combination of innovative molecular markers were used to infer past fires, vegetation, and human interactions in sediment cores analysed from Guatemala (Schüpbach et al., 2015) and East Africa (Battistel et al., 2016).Using a similar approach, we use biomarkers that are produced under specific environmental conditions and then transported, accumulated, and stored in lacustrine sediments: monosaccharide anhydrides (MAs); fecal sterols and stanols (FeSts); polycyclic aromatic hydrocarbons (PAHs); and normal(*n*)-alkanes. Significant concentrations of these compounds are present in soil and sedimentary archives with ages older than 10 cal ky BP (D'Anjou et al., 2012; Johnsen et al., 2005; Schüpbach et al., 2015), suggesting that degradation, if happening, is a low-kinetic process (Battistel et al., 2016) and that these compounds resist over the Holocene or longer timescales. Within the listed biomarkers, MAs are specific tracers of vegetation combustion (Simoneit, 2002; Zangrando et al., 2013). Cellulose pyrolysis creates the molecular marker levoglucosan (1,6-anhydro-β-D-glucopyranose) (Simoneit et al., 1999), while hemicellulose combustion produces the isomers mannosan (1,6-anhydro-β-D-mannopyranose)

and galactosan (1,6-anhydro-β-D-galactopyranose) (Kuo et al., 2011). Several studies examine levoglucosan (L), mannosan (M) and galactosan (G) in aerosols and ice cores (Kehrwald, 2012; Simoneit, 2002; Yao et al., 2013; Zennaro et al., 2014; Zhang et al., 2008), as well as in sediment cores (Battistel et al., 2016; Kirchgeorg et al., 2014; Schüpbach et al., 2015), demonstrating the suitability of MAs as paleofire proxies. PAHs are a wide group of organic compounds made up of two or more benzene rings combined together in linear, angular, or clustered arrangements (Zakir Hossain et al., 2013). The physical properties of PAHs, such as low aqueous solubility and high lipophilicity, prevent microbial utilization and promote their accumulation as particulates in terrestrial environments (Johnsen et al., 2005). This class of molecules is produced by incomplete combustion during a wide range of natural and anthropogenic processes, such as volcanic eruptions, vegetation and/or garbage burning, fossil fuels, and cigarette or car emissions (Abdel-Shafy and Mansour, 2016; Kim et al., 2013; Lima et al., 2005). PAHs are semi-volatile, persistent, and ubiquitous in the environment with multiple possible sources, and therefore commonly detected in soil, air, and water (Abdel-Shafy and Mansour, 2016; Johnsen et al., 2005). The investigation of PAHs as tracers of biomass burning in past climate archives such as sediments (Jiang et al., 1998) and ice (Gabrieli et al., 2010) is increasing in the last decades (Yan et al., 2014; Page et al., 1999).

Leaf waxes are preserved in sediments and can help determine past vegetation in a lake catchment. The cuticular wax layer of terrestrial plants consists predominantly of long-chain hydrocarbons (n-alkanes) and creates a protective barrier that helps maintain the plant's integrity within an intrinsically hostile environment (Sheperd and Griffiths, 2006). The leaf wax of higher plants is assumed to be stable, and is difficult to degrade during transport, deposition, and burial (Cui et al., 2008). Different types of plants have diverse distribution of n-alkanes chain-lengths (Diefendorf and Freimuth, 2017). Angiosperms generally produce more n-alkanes than gymnosperms; however, chain-length distributions are highly variable within plant groups, and especially for conifers where the Cupressaceae group tends to have long chain n-alkanes, while the Pinaceae group tends to have relatively short chain n-alkanes (Diefendorf and Freimuth, 2017; Diefendorf et al., 2015). *Sphagnum* mosses are among the few plants that provide a characteristic signal as these mosses are marked by the predominance of C_{23} and C_{25} (Bush and McInerney, 2013). Long chain n-alkanes (C_{27}–C_{33}) with a strong odd/even predominance are usually interpreted to be of terrestrial origin; mid-chain n-alkanes (C_{20}–C_{25}) are mainly present in aquatic macrophytes; bacteria, algae and fungi primarily produce short chain n-alkanes in the range C_{14}–C_{22}, while n-C_{17} is an indicator for algae and photosynthetic bacteria (Aichner et al., 2010; Ficken et al., 1998; Grimalt and Albaigés, 1987; Han and Calvin, 1969). Due to the large range of possible chain lengths present within sediments, ratios of n-alkanes are often used to determine the vegetation composition. The most commonly used ratios are the average chain length (ACL) (Poynter and Eglinton, 1990), the carbon preference index (CPI) (Bray and Evans, 1961), the submerged versus emergent aquatic plants predominance ratio (P_{aq}) (Ficken et al., 2000), and the grass to wood prevalence ratio (Norm31) (Carr et al., 2014). However, it is still unclear to what extent variations in leaf wax composition within paleoenvironmental archives can be explained in terms of changes in the relative proportions of different plant species on the landscape and/or the reaction of a plant community to environmental conditions (Carr et al., 2014).

Revealing human presence in lake catchments often relies on anthropological evidence, but advances in proxy development during the past two decades now allows determining the presence of humans or pastoralism through steroid fecal biomarker concentrations (Bull et al., 2002). FeSts, such as stanols and bile acids, in lake sediments reflect grazing in a lacustrine catchment (D'Anjou et al., 2012). Specific FeSts, such as 5β-stanols, are organic compounds produced by the microbially mediated alteration of cholesterol in the intestinal tracts of most mammals, making them ideal fecal biomarkers (Dubois and Jacob, 2016). Coprostanol and stigmastanol derive from hydrogenation of cholesterol and stigmasterol by bacteria present in the intestines of humans or animals and can indicate human presence and animal husbandry, respectively (Daughton, 2012; Vane et al., 2010). These molecules are also used as chemical indicators of fecal pollution of lakes, rivers, and drinking water (Daughton, 2012; Vane et al., 2010; Wu et al., 2009). In addition, FeSts can originate from vegetation, e.g. β-sitosterol is synthesised by higher vascular plants (Nishimura and Koyama, 1977; Vane et al., 2010) and its derivative β-sitostanol is generated from a reduction reaction in sediments (Martins et al., 2007).

In this study, we reconstruct fire activity and vegetation changes using a multi-proxy analytical approach applied to lacustrine sediment samples from the south-eastern Tibetan Plateau. This is the first study to combine MAs, PAHs, *n*-alkanes and FeSts analyses into a single analytical method highlighting the interactions between fire, climate, and vegetation during the Holocene. This combination of proxies, when synthesized with regional climate records, helps determine the changing role of local and regional fire activity throughout the Holocene.

2 Study Area, Modern Climate, and Holocene Climate History

The Qinghai-Tibetan Plateau is a vast plateau in central Asia with an average elevation of approximately 4500 m above sea level (asl). The TP stretches nearly 1000 km north to south and 2500 km east to west, covering an area of 2×10^6 km^2 (Dong et al., 2010). In addition to this wide geographic range, the TP also encompasses altitudes ranging from 1500 to > 8000 m asl, resulting in highly heterogeneous landscapes with considerable biodiversity. In general, however, vegetation across much of the TP is dominated by meadow, steppe, and shrub communities where species richness increases with increasing altitude (Shimono et al., 2010). The TP is a pivotal research area due to its sensitivity to century-scale or short-term climatic changes and its influence on global climate (Liu et al., 1998). However, its remote nature restricts access to possible paleoclimate studies, resulting in relatively few investigations of past species diversity and plant community changes (Wang et al., 2006).

The TP's climate is regulated by the critical and sensitive junction of four climatic systems (Supplement S1): the Westerlies; the East Asian Monsoon; the Siberian cold polar airflow (or Winter Monsoon); and the Indian Monsoon (Dong et al., 2010). Westerly winds and the Indian Summer Monsoon (ISM) are considered to be the major wind patterns by which atmospheric particulates derived from biomass burning reach the plateau (Yao et al., 2013). Millennial-scale changes in insolation over the TP affect monsoon variability and the associated moisture reaching the TP. Generally, during periods of increased insolation, the monsoon extended farther north on the TP, resulting in more vegetation growth across the plateau. During decreased

insolation, colder, drier conditions dominate the TP and regions influenced by the ISM are restricted to more southerly portions of the plateau, including the study area. During the late Pleistocene (~ 16 cal ky BP), a cold and dry climate resulted in desert-steppe vegetation across much of the TP (Tang et al., 2000). Global paleoclimate studies indicate that this last glacial period concluded with a sudden warming event at ~ 15 cal ky BP (Severinghaus and Brook, 1999), in the context of Bølling–Allerød and Younger Dryas events in the region (Liu et al., 2008). The subsequent transition to the Holocene was characterized by increasing temperature and precipitation that enhanced permafrost and snow melting and facilitated tree growth in the TP after 12 cal ky BP (Saini et al., 2017; Tang et al., 2000). This period was depicted by frequent oscillations between warm and cold phases, in Tibet as well as in other parts of the world (Liping Zhu et al., 2008; Liu et al., 2008, 2009). For example, Tang et al. (2000) suggest that the evolution of the ISM has considerably fluctuated throughout the Holocene. Lake Ximencuo (eastern Tibet) sediments record cold events occurring between 10.3–10.0, 7.9–7.4, 5.9–5.5, 4.2–2.8, 1.7–1.3 and 0.6–0.1 cal ky BP, where the cold event at 4.2 cal ky BP had the most substantial impact (Miao et al., 2015; Mischke and Zhang, 2010). Superimposed on these oscillations, the general temperature trends affecting the TP include a warm and humid climate in the early to mid-Holocene, as registered in sediments and dust deposits (Liu et al., 2008), and then a cooling trend during the mid-Holocene. The high temperatures during the early Holocene accelerated evaporation and caused many Tibetan lakes to evolve from open freshwater systems to saline lakes (Dong et al., 2010), despite increased monsoonal precipitation (Bird et al., 2014). TP vegetation also responded to these warmer temperatures with an increase in forests and forest-meadows between 9.2 and 6.3 cal ky BP (Tang et al., 2000). During the mid to late Holocene, warm-wet conditions shifted towards a cooler and drier climate, due to weaker solar insolation, and after 5 cal ky BP temperature and precipitation decreased linearly (Bird et al., 2014; Dong et al., 2010; Liu and Feng, 2012; Tang et al., 2000). More recently, human activities and related climate change have significantly altered the regional hydrology and vegetation distribution of the plateau, with flora degeneration that led to desertification and frequent dust storms (Wang et al., 2008).

Paru Co (0.1 km^2) is located in the Nyainqentanglha Mountains (29°47'45.6"N, 92°21'07.2"E; 4845 m asl; Figs 1a and 1b) and is dammed by moraines from past glaciations in its watershed. The biome surrounding Paru Co is temperate subalpine steppe, where the lake is located near the border of alpine coniferous forest and tropical and seasonal rainforests (Li et al., 2016). The lake's watershed is 2.97 km^2 and consists of a sloping glacial valley measuring 0.5 to 2.0 km in length with lateral mountain crests higher than 5000 m asl. The maximum water depth of the modern lake is 1.2 m, with gently sloping sides, but may tolerate a total water level of about 3 m. A central ephemeral stream channel and a second incised channel drain the lake's watershed and feed Paru Co with runoff. Outflow from the lake drains via a small stream channel located approximately 430 m west of the primary outlet (Bird et al., 2014). The Tropical Rainfall Measuring Mission data (TRMM) from 1998 to 2007 show that approximately 92% of mean annual precipitation (MAP; 1118 mm y^{-1}) at Paru Co occurs between April to September during the ISM season (Fig. 1c, Bird et al., 2014). Previous paleoclimate work at Paru Co (Bird et al., 2014) indicates the occurrence of intense ISM rainfall between 10.1 and 5.2 cal ky BP, when five-century-long high lake levels were recorded. The ISM weakened after ~ 5.2 cal ky BP, with the exception of a pluvial event centred at 0.9 cal ky BP. Nir'pa Co, a small

lake located near Paru Co, suggests a wet period between 3.3 and 2.4 cal ky and drier conditions from 2.4 to 1.3 cal ky, due to lower silt and lithic content, coincident with elevated sand and clay content and lower lake levels (Bird et al., 2017).

3 Methods

3.1 Coring and chronology

5   Paru Co core B11 was collected in 2011 and extends from 0 to 435 cm. Seven radiocarbon ages determined by accelerator mass spectrometry (AMS ^{14}C) were measured on seven carbonized grass fragments extracted from the surrounding sediments (Bird et al., 2014). The sedimentation rate is approximately 0.35 mm y^{-1} between 10.768 cal ky BP and the present. Between 10.937 to 10.789 cal ky BP sedimentation rates are approximately 10 times higher (3.3 mm y^{-1}). The final age-depth model (Fig. 1d) was constructed using a linear regression between 434.9 and 364.1 cm and by fitting a 3rd order polynomial to the

10   AMS ^{14}C, ^{137}Cs (-0.013 cal ky – determined by direct gamma counting) and sediment-water interface (-0.061 cal ky) ages between 364.1 and 0.0 cm. The associated model error is between 15 and 90 years (see Bird et al. (2014) for further details). As the deepest part of the core shows a much higher sedimentation rate that cannot be clearly explained, with the possibility of data distortion, the subsequent description and discussion of the results exclude the samples with ages between 10.784 and 10.937 cal ky BP, limiting the dataset interpretation to the period between 1.347 and 10.768 cal ky BP.

15   ### 3.2 Sample preparation

Sub-samples (n = 72) were selected from the core every 5 cm, spanning from 10.9 to 1.3 cal ky BP with a time resolution of about 130 years on average. Unfortunately, the uppermost samples covering the more recent period (1.3 – 0 cal ky BP) have not been processed for this study due to lack of sufficient sample amounts. The samples were sealed in plastic bags and stored at -20 °C, weighed, freeze-dried and ground and reweighed in order to assure ~ 1 g of dry material, allowing the possibility of

20   determining MAs, PAHs, n-alkanes, and FeSts from the same sample. All samples were ground using a Mixer Mill MM 400 (Retsch GmbH, Germany) ball miller.

The 72 Paru Co samples were extracted with a 9:1 v/v mixture of ultra-grade (Romil Ltd., Cambridge, UK) dichloromethane and methanol (DCM:MeOH) with a Thermo Scientific Dionex ASE 350 (Accelerated Solvent Extractor system), in order to extract both the polar and non-polar compounds. For each extraction, we used 22 mL steel cells containing a 27 mm ø cellulose

25   filter, diatomaceous earth, the sample, ~ 2 g of Na$_2$SO$_4$ (to remove residual moisture) and ~ 2 g of activated copper (to remove sulphur that can interfere with PAHs analysis). We added the following internal standard solutions into each cell: 100 μL of ^{13}C labelled levoglucosan at 1 ng μL^{-1} of concentration, 100 μL of hexatriacontane at 40 ng μL^{-1}, 100 μL of a mixture of ^{13}C labelled PAHs (acenaphthylene, phenanthrene, and benzo[a]pyrene) at 1 ng μL^{-1}, 100 μL of cholesterol-3,4-^{13}C$_2$ at 1 ng μL^{-1}. The extractions were performed with three static cycles at 100 °C and 1500 psi. A procedural blank was created and extracted

30   for every batch of 12 samples, where we filled the steel cell with all of the same reagents, but without a sample.

Each sample was then purified with three steps to obtain a PAHs/*n*-alkanes fraction, a FeSts fraction, and a MAs fraction. We combined and modified published clean-up methodologies in order to obtain the necessary fractions (Battistel et al., 2015; Douglas et al., 2012; Kirchgeorg et al., 2014; Martino, 2016). Our resulting method uses 12 mL Solid-Phase Extraction cartridges (SPE DSC-Si 10 Tube; 12 mL; 52657 Supelco, Sigma-Aldrich) packed with 2 g of silica gel (particle size 50 µm)

5   and installed on Visiprep™ (SPE Vacuum Manifold standard, Sigma-Aldrich) to accelerate purification. We conditioned each cartridge with 30 mL of DCM and 30 mL of Hexane (Hex). The first non-polar fraction (F1), containing PAHs and *n*-alkanes, was eluted using 40 mL of a Hex:DCM 9:1 v/v mixture. Then, the second polar fraction (F2), containing FeSts, was separated with 70 mL of DCM. This fraction was derivatized, according to Battistel et al. (2015), at 70 °C for 1 h with 100 µL of BSTFA + 1% TMCS (N,O-bis(trimethylsilyl)trifluoroacetamide with 1 % trimethylchlorosilane, Sigma-Aldrich) to increase compound

10 volatility and detectability during gas chromatography – mass spectrometry (GC-MS) analysis. Finally, the third polar fraction (F3) containing MAs was eluted with 20 mL of MeOH. F1 and F2 were evaporated under a stream of pure N_2 using a TurboVap II® system (Caliper Life Science, Hopkinton, MA, USA) in order to reduce the volume to 150 µL. F3 was dried, dissolved in 0.5 mL of ultra-pure water and sonicated to avoid any adsorption of MAs to walls of glass evaporation tubes. Finally, the samples were centrifuged (5 min, 14000 rpm) and transferred using decontaminated Pasteur pipettes to the measurement vials.

15 ### 3.3 Sample analysis

MAs were detected using methods published in Kirchgeorg et al. (2014) with ion chromatography (IC Dionex ICS 5000, Thermo Scientific, Waltham, USA) coupled with a single quadrupole mass spectrometer (MSQ Plus™, Thermo Scientific) equipped with CarboPac MA1™ column (Thermo Scientific, 2 x 250 mm) and an AminoTrap column (2 x 50 mm), resulting in a good separation of the isomers levoglucosan, mannosan and galactosan. The injection volume was 50 µL. A solution of

20 MeOH/NH_4OH was added post-column (0.025 mL min^{-1}) to improve ionization of the aqueous eluent before entering the electrospray ionisation (ESI) in negative mode. The analytes were quantified according to specific mass to charge ratios, and with calibration curves and response factors containing unlabelled molecules of L, M, G, as well as an internal standard molecule (^{13}C labelled levoglucosan).

The 17 priority PAHs (according to US ATSDR, 1995) plus retene, *n*-alkanes (from C_{10} to C_{35}) and FeSts (coprostanol, epi-

25 coprostanol, cholesterol, 5α-cholestanol, sitosterol, sitostanol) were analysed with gas chromatography (6890-N GC system) coupled to a single quadrupole mass spectrometer (MS 5975, Agilent Technologies, Santa Clara, CA, USA) (Argiriadis et al., 2014; Battistel et al., 2015; Gregoris et al., 2014; Martino, 2016; Piazza et al., 2013). Each analysis used the same capillary column (HP5-MS (5%-phenyl)-methylpolysiloxane, Agilent Technologies, Santa Clara, CA, USA). The conditions were an injection volume of 2 µL (split valve open after 1.5 min) and He as a carrier gas (1 mL min^{-1}). The MS was equipped with an

30 electronic ionization (EI) source used in positive mode. The analytes were quantified in single ion monitoring mode (Table 1). We created response factors containing all of the target compounds as well as internal standards (^{13}C labelled acenaphthylene, phenanthrene and benzo[a]pyrene at 1 ng µL^{-1} - Cambridge Isotope Laboratories, Inc; hexatriacontane at 40 ng µL^{-1} and

cholesterol-3,4-^{13}C$_2$ at 1 ng µL^{-1} - Sigma Aldrich). We ran a response factor after every seven samples in order to monitor possible instrumental drift, as well as running a full calibration curve of external PAH standards before each set of analyses.

Target molecules with their respective analysed ions and method detection limits (MDL) are listed in Table 1. Further method details and quality assurance are available in previously published work (Argiriadis et al., 2014; Battistel et al., 2015; Gregoris et al., 2014; Kirchgeorg et al., 2014; Martino, 2016; Piazza et al., 2013). Chromatographic peak identification and calculations were performed using the Chromeleon™6.8 Chromatography Data System Software (Thermo Scientific, Waltham, USA) and Agilent G1701DA GC/MSD ChemStation (Agilent Technologies, Santa Clara, CA, USA).

3.4 Data Analysis

All concentration values obtained from IC and GC-MS analyses were converted to ng g^{-1} or µg g^{-1}, and then transformed into fluxes in order to correct the data for the influence of time and sedimentation. Fluxes (ng cm^{-2} y^{-1}) were calculated by multiplying the sedimentation rate (cm y^{-1}), wet density (g cm^{-3}) and concentration (ng g^{-1}) of the respective analyte (Menounos, 1997). As explained in Section 3.1, we investigate the data between 1.347 and 10.768 cal ky BP which has a constant sedimentation rate. The concentrations of each analyte therefore have the same trends as their resulting fluxes (Supplement S2). We present all results as concentrations (ng g^{-1} or µg g^{-1}).

N-alkane ratios useful for our study include: the average chain length (ACL), representing the composite of longer and shorter *n*-alkanes between the chain length range of 21 to 33 and indicating the weighted predominant length (Poynter and Eglinton, 1990); the carbon preference index (CPI), an expression of odd/even predominance that represents how much of the original biological chain length specificity is preserved in geological lipids (Meyers and Ishiwatari, 1993); and the P-aqueous ratio (P_{aq}), that helps differentiate between submerged plants that tend to have medium-chain-length *n*-alkanes and terrestrial plants that tend to have longer chain lengths (Ficken et al., 2000). These ratios were calculated according to the following equations:

(1) $$ACL_{21-35} = \frac{\sum (n_{21-35})(C_{21-35})}{\sum (C_{21-35})}$$

(2) $$CPI_{21-33} = \frac{1}{2} \frac{\sum C_{odd(21-33)} / \sum C_{even(20-32)}}{\sum C_{odd(21-35)} / \sum C_{even(22-34)}}$$

(3) $$P_{aq} = (C_{23} + C_{25})/(C_{23} + C_{25} + C_{29} + C_{31})$$

where n$_{21-33}$ indicates the number of carbons in the *n*-alkane chains and C$_n$ represents the concentration of the respective *n*-alkane. In order to help data interpretation, 2-tailed Pearson's correlations were calculated in R for the biomarkers dataset with a 95% confidence interval (Supplement S3) with statistically significant results when p-values are < 0.05.

4 Results

4.1 Paleofire indicators

MA concentrations values span from 29 to 6497, from 15 to 993 and from 17 to 1722 ng g^{-1} for levoglucosan, mannosan and galactosan, respectively. In the most recent sample from 1347 cal ky BP, none of the three MAs were above the detection limits while in a few other samples mannosan and galactosan were below the MDL. The Paru Co MA results reflect the general observation in the literature that mannosan and galactosan concentrations are almost always less than levoglucosan concentrations, which may be due to the different thermal stability of their respective precursors, hemicellulose and cellulose (Kuo et al., 2011; Simoneit, 2002). Although levoglucosan (Fig. 2e) and galactosan may have different precursors, their trends throughout the Paru Co core are generally similar, while peaks in mannosan (Fig. 2f) concentrations differ slightly from the other two isomers. The MA signal is much higher during the early Holocene (10.8-8 cal ky BP) and then slightly increases again during the periods 7-5 and 3-2 cal ky BP.

The lowest PAH value is 0.2 ng g^{-1} of benzo[b]fluoranthene (BbFl) while the highest PAH concentration is 310.3 ng g^{-1}, of naphthalene (Naph). Phenanthrene (Phe), benzo[e]pyrene (BePyr) and Naph respectively represent 20.9%, 18.9% and 17.5% of the total PAH signal in Paru Co (please see Supplement S4 for single PAHs concentrations). The total sum of PAHs (∑PAHs – Fig 2a) shows higher values in the middle Holocene, with major peaks at 6.3, 5.8, 5.2, 4.8, 3.9 and 3.5-3.3 cal ky BP. The general trend shows increases from 2.2 to 1.3 cal ky BP. The molecular weight and/or number of aromatic rings of PAHs allows investigating the influence of different PAH types through time. The group of 3ring-PAHs (Fig. 2b) includes Phe, anthracene (Ant) and fluoranthene (FluA), demonstrating a similar pattern to the ∑PAHs. The group of 4ring-PAHs (Fig. 2c) encompasses pyrene (Pyr), benzo[a]anthracene (BaAnt), chrysene (Chr), retene (Ret), benzo[b]fluoranthene (BbFl) and benzo[k]fluoranthene (Bkfl), which also has higher values during the middle Holocene and then an increasing trend towards 1.3 cal ky BP. The group of 5-6ring-PAHs (Fig. 2d) is composed of benzo[a]pyrene (BaPyr), BePyr, benzo[ghi]perylene (Bghi), Indeno[1,2,3,-c,d]pyrene (IP) and dibenzo[a,h]anthracene (DBahAnt), with a more noisy trend and dissimilar behaviour from the rest of the groups. 5-6ring-PAHs are high in the early Holocene, peaking at 10.3-9.9 cal ky BP, and then have separate high concentrations at 9.3, 8.6, 7.2, 5.2, 3.9, 3.5, 2, and 1.3 cal ky BP.

The ratios of both MAs and PAHs help reconstruct past vegetation and burning sources. MA ratios can help determine past vegetation types and/or burning temperatures. High combustion temperatures (~ 300 °C) and longer combustion durations result in higher L/M and L/(M+G) ratios, regardless of plant species (Kuo et al., 2011). The L/M and L/(M+G) ratios in Paru Core range from 0.6 to 100 and 0.5 to 11.1, respectively (Supplement S5). The L/M ratios peak between ~ 6 and 7 cal ky BP, with the highest value of 98.8 (Fig. 3a). The L/(M+G) values do not peak at the same time, but oscillate throughout the Holocene, with the highest values centred around ~ 2 cal ky BP. Although MA ratios cannot precisely point to the type of past burnt vegetation, these ratios can classify general vegetation types (Fabbri et al., 2009). However, due to the fact that galactosan presents a different biodegradation behaviour, the application of L/(M+G) ratio may be inadequate (Kirchgeorg, 2015). For

this reason, we limited the discussion only to L/M ratio results.

PAH diagnostic ratios used in this study are Ant/(Ant+Phe), IP/(IP+Bghi) and FluA/(FluA+Pyr). Ant/(Ant+Phe) values generally discriminate between petroleum (< 0.10) and combustion (> 0.10) sources; IP/(IP+Bghi) distinguishes between different combustion sources, with values > 0.5 for grass, wood or coal combustion, values between 0.2 and 0.5 for liquid fossil fuel combustion and values < 0.2 for petroleum sources; FluA/(FluA+Pyr) is used to define the transition point (0.5) between petroleum and combustion (Denis et al., 2012; Yunker et al., 2002a; Yunker et al., 2002b; Yunker et al., 2015; Zakir Hossain et al., 2013). In Paru Co these ratios are plotted with absolute error bars (Fig. 2-g,h,i), in order to highlight that the influence of error propagation from the original analysis to the ratio values should be carefully investigated (Hughes and Hase, 2010) when assigning sources from the ratios. Considering the error bars, the three ratios shows values > 0.10 for Ant/(Ant+Phe), > 0.5 for IP/(IP+Bghi) and > 0.5 for FluA/(FluA+Pyr) for the majority of the analysed samples.

4.2 Vegetation and human indicators

The variations in n-alkane ratios help reconstruct past vegetation changes, as n-alkanes record the organic input into and within the lake. The n-alkane concentrations oscillate between 0.6 ng g^{-1} (C10) and 321 µg g^{-1} (C25) with C25 as the most abundant (39.8%) followed by C27 (15.8%) and C29 (9.2%). ACL$_{21-35}$ values fluctuate between 24.9 and 27.9, with a general decreasing trend from 10.8 cal ky BP till 7.2 cal ky BP and then an increasing pattern until 1.3 cal ky BP (Fig. 4b). P$_{aq}$ ratios (Fig. 4c) vary between 0.3 and 1 with a trend that is the opposite of ACL$_{21-35}$. CPI$_{21-33}$ demonstrates a general predominance of odds over evens, with values < 1 only occurring in three cases (1.8, 3.2, 8.6 cal ky BP) and where the maximum value of 41.2 happens at 10.1 cal ky BP (Fig 3b).

FeSts contain very low values for the majority of the analysed compounds. Only three FeSts are above the MDL in Paru Co, but these FeSts are not quantifiable in all samples. These FeSts include sitostanol (5α-Sit) that represents 58% of the quantifiable total, sitosterol (Sit) with 37% and cholestenol (5α-Ch) with only 3% of the total. The maximum FeSt concentration throughout the entire core is from 5α-Sit (282 ng g^{-1}) at 2 cal ky BP (Supplement S7). Due to the generally low concentrations, no diagnostic ratios were calculated for the FeSts.

5 Discussion

5.1 Paleofire activity

It is not always easy to distinguish the pyrogenic, biogenic and petrogenic sources of PAHs in a specific place because: i) the same compound can be derived from different sources, ii) PAH profiles depend on the combustion temperature, the duration of the process, the flame conditions (oxygen) and the type of organic material (Daly et al., 2007) and iii) once deposited, PAHs undergo transformation processes that depend on the chemical characteristics of the compounds and environmental variables

(Cai et al., 2008; Ma et al., 2005; Maliszewska-Kordybach et al., 2009). Taking these conditions into account, we interpret the PAH profiles in Paru Co as fire-related as no evidence of other sources (e.g. volcanic eruptions, anthropogenic emissions) was found.

During the early Holocene (10.8-8.5 ky BP) levoglucosan, galactosan, mannosan and 5rings-PAHs show similar trends, with a general decreasing pattern and some higher peaks at 10.5-10, 9.2 and 8.5 cal ky BP. During the middle Holocene fires are recorded between 6.5-4 cal ky BP by levoglucosan, and more evidently by PAHs spikes. The late Holocene shows increasing PAHs from 3 to 1.3 ky BP with levoglucosan peaks at ~ 2 ky BP (Figs 2-a,b,c,d,e,f).

The high concentrations of higher molecular weight PAHs during the early Holocene could be explained with local fires of greater combustion temperatures, due to the fact that higher number of rings requires greater burning energy (Denis et al., 2012). High percentages of 4-6 ring PAHs generally suggest the contribution of local high-temperature combustion origins (Yang et al., 2016), where such combustion may be the source of BePyr, the congener with the second highest concentration in Paru Co, but also of IP and Bghi, which are high temperature markers (Zakir Hossain et al., 2013). When fuel sources are uniform, hotter fires (at and above 500 °C) commonly produce high concentrations of BePyr, IP, Bghi (McGrath et al., 2003; Zakir Hossain et al., 2013). The lower, but not lacking, presence of 3rings and 4rings-PAHs could be due to the fact that lower molecular weight PAHs are more depleted due to weathering processes (Zakir Hossain et al., 2013). Their lower concentrations may also be due to the fact that the 3ring and 4ring-PAHs could have travelled farther since they are more volatile than the 5-6 ring PAHs. In addition, the 3ring and 4ring-PAHs may have photochemically degraded in the gas phase after emission to the atmosphere (Wang et al., 2010).

Higher molecular weight PAHs are more stable compounds compared to 3-4 ring PAHs. If we assume that low molecular weight PAHs degrade at 500 °C, we have to assume that MAs may also degrade at this temperature, as maximum concentrations occur at burning temperatures centred around 250 °C (Zennaro et al., 2015 and references therein). In the Paru Co record, levoglucosan concentrations are higher than PAHs during the early Holocene. Therefore, in order to explain this discrepancy, regional early Holocene fires must have been more frequent than local fires, producing high amounts of MAs, without excluding that atmospheric transport of levoglucosan to Paru Co was more efficient during the early Holocene. Therefore, this high abundance of levoglucosan may also be related to a regional signal, as MAs are capable of travelling hundreds of kilometres (Schüpbach et al., 2015; Zennaro et al., 2014).

MAs continue to decrease from 8.5 ky BP to 1.5 ky BP whereas 3, 4, and 5 ring-PAHs start increasing before reaching their greatest values between 6.5 and 4 ky BP (Figs 2-b,c,d,e,f). This difference may due to higher percentages of lignin burning (evidenced by retene peaks – Supplement S6) with respect to cellulose burning (represented by MA concentrations). Pollen profiles (Zhao et al., 2011) indicate an increased presence of trees between 7 and 3 ky BP. The combination of low concentrations of the 5-6 ring PAHs but abundant FluA, Pyr and BePyr suggests geographically small, but more frequent

wildfires (Zakir Hossain et al., 2013). We interpret the Paru Co record between 6.5 and 4 cal ky BP as the result of such relatively small, but recurrent fires.

The explanation for the lack of levoglucosan and other MA peaks during the period of the highest concentrations of PAHs (6.5-3 cal ky BP) may be due to: i) different burning temperatures and conditions, i.e. MAs are produced in smouldering and low temperature fires while high temperature flaming fires produce PAHs (Simoneit, 2002); ii) the lipophilic properties of PAHs, which have a low solubility in water (Haritash and Kaushik, 2009) while levoglucosan has a relatively higher water solubility, with an estimated half-life time of 5-8 days due to possible degradation from aquatic microorganisms who utilize the "free" form of levoglucosan (Norwood et al., 2013). Increased presence of PAHs may also be due to the sedimentation itself. PAHs derived from pyrogenic sources generally associate with soot-rich particles that protect them from degradation in the atmosphere, water column and sediments (Yunker et al., 2002b). PAHs from forest fires only travel relatively local distances but are protected from photolytic degradation due to their association with larger particles, helping them survive the transport from the atmosphere into climate archives such as sediments (Yunker et al., 2002b).

5.2 Combustion sources

The diagnostic ratios and associated error propagation (Figs 2-g,h,i) do not allow quantitatively assigning PAH sources. IP/(IP+Bghi) contains values above the 0.5 threshold for combustion of wood, wood soot and/or grasses, creosote, as well as almost all wood and coal combustion aerosols and bush fire (Yunker et al., 2002b). The FluA/(FluA+Pyr) ratio, with values above 0.5 for the majority of the samples, indicates the combustion of grass, wood or coal, although this threshold is not definitive (Yunker et al., 2002b). The Ant/(Ant+Phe) ratio with values > 0.10 is generally related to pyrogenic PAH sources, but overlapping values between petroleum and combustion sources are reported (Yunker et al., 2002b). In Paru Co, when including the error propagation, the majority of samples show values of Ant/(Ant+Phe) > 0.10. Due to the improbability that petroleum sources were burned near Paru Co during the geological time period covered by the analysed core, the obtained values for the ratio Ant/(Ant+Phe) must be related to vegetation combustion. In general, Ant undergoes more rapid photochemical reactions in the atmosphere than Phe. In contrast, FluA/Pyr and IP/Bghi isomer pairs degrade at comparable rates and the original composition information is preserved during atmospheric transport (Yunker et al., 2002b) suggesting that their ratios may be more reliable compared to the Ant/(Ant+Phe) ratio. Given these considerations, we confirm that diagnostic ratios are important tools for the source assignment but cannot be completely trusted due to overlapping values and error propagation that may hinder the correct allocation of the signal origin. However, PAHs in Paru Co can function as pyrogenic markers as we did not find any evidence of other sources (e.g. volcanic eruptions, anthropogenic emissions).

The sum of PAH concentrations demonstrates similarities to the eastern TP tree pollen record from the Zoige basin (Fig. 3; Zhao et al., 2011). The Zoige basin is 450 km to the north-east of Paru Co and, in addition to Hidden Lake (Tang et al., 2000), are among the closest pollen records to Paru Co. Both records demonstrate Holocene vegetation fluctuations in the region and

are consistent with other pollen and modelling studies (Dallmeyer et al., 2011; Herzschuh et al., 2006; Lu et al., 2011), which identify decreasing summer monsoon precipitation and changes in warm season temperature as the mechanisms responsible for the vegetation shifts from meadow to conifer forest to alpine steppe. The average forest fraction on the TP shrank by almost one-third from the mid-Holocene (41.4%) to the present (28.3 %). Shrubs quadrupled in their mid-Holocene percentage to present-day (12.3 %), replacing much of this forest. The grass fraction also increased from 38.1% during the mid-Holocene to the current percentage of 42.3% (Dallmeyer et al., 2011). This forest decline and replacement by shrubs from 6 cal ky to present is prevalent across much of the south-eastern TP (Lu et al., 2011).

PAHs values are low in the early Holocene where, instead, tree pollen values are quite high. However, in the mid-Holocene PAHs contain higher concentrations from 6.5 cal ky BP, concurrent with a peak in the percentage of tree pollen. The subsequent decreasing trend in tree pollen, from 4.7 cal ky BP onward, is associated with a drying and cooling climate that may have intensified fire as recorded by PAHs in Paru Co, creating a positive feedback resulting in even more decreasing tree coverage. This decreasing trend in tree pollen reaches its lowest values after 3 cal ky BP. The regional wetter climatic conditions during the early and mid-Holocene (Bird et al., 2014; Tang et al., 2000) may have favoured forest expansion, where this biomass became available for successive burning during the more arid climate of the late Holocene, when PAHs show an increasing trend (Fig. 2a).

In addition to the PAH ratios, L/M ratios can also help determine combustion sources (Fig. 3a). L/M emission ratios ranging between 0.6–13.8 may be due to softwood combustion, while ratios between 3.3–22 depict hardwood burning, and ratios 2.0–33.3 may be due to burning grasses (Fabbri et al., 2009 and references therein). Therefore, the Paru Co data suggest that the fire signal from MAs after 10.74 cal ky BP is likely due to conifer burning in the region. Successively, grasses, softwood and hardwood burning oscillated until 8.6 cal ky BP, where hardwood combustion prevailed until 7.7 cal ky BP, followed by the predominance of grassland burning. Although MA ratios can generally differentiate between grass versus wood burning (Kirchgeorg et al., 2014), specific L/M and/or L/(M+G) ratios do not directly correspond to individual fuel types (Matsubara Pereira, 2017) due to the problem of overlapping ratios and similar burning conditions that influence the ratios.

In order to obtain more information from the burning conditions, we compared CPI values to L/M and PAHs (Fig. 3). Considering that PAHs and n-alkanes are both local indicators, variations in CPI corresponding to spikes in local fire markers may link combustion and vegetation types demonstrated by *n*-alkane abundances. While no correlation exists between PAHs and CPI, the CPI and L/M have a slight positive correlation (r = 0.31, p-value = 0.03). Medeiros and Simoneit (2008) found that the *n*-alkanes in green vegetation smoke contained distributions ranging from C_{23} to C_{35}, with strong odd-to-even carbon number predominance evidenced by CPI ranging from 9 to 58. MAs are better at recording smouldering fires than are PAHs, which may in part explain the similarity between MA and CPI variability through time. The Paru Co CPI values peak around 10 cal ky BP, in the period between 7.8 and 3.5 cal ky BP, and at 2.3 cal ky BP, with values up to 41.2, similar to the peak distributions of L/M. Another argument for the relationship between CPI and MAs fire is the fact that lower temperature fires

(MAs) essentially steam-distil the vascular plant lipids into the smoke, while high-temperature fires (PAHs) can result in decrease of the CPI, potentially due to the thermal generation of *n*-alkanes of lower CPI from macromolecular material (Schefuss et al., 2003; Standley and Simoneit, 1987). In addition, the distance from the vegetation to the sediments may influence the CPI record as plants that are in or near the water pools contain shorter carbon chains, whereas more distant plants

5   have higher CPI values (García-Alix et al., 2017). Using these considerations, we assume that when CPI and L/M are parallel to each other, they record both fire from the surrounding areas as well as from near the lake catchment.

5.3 Vegetation in the lake catchment

Past vegetation changes can also be derived from variations in *n*-alkane ratios, as *n*-alkanes can record the organic input into and within the lake. The average chain length (ACL) represents the composite of longer and shorter *n*-alkanes (Poynter and

10 Eglinton, 1990), encompassing the chain length range of 21 to 35. The peak in ACL_{21-35} values at 10.9 – 10 cal ky BP may reflect fewer submerged aquatic plants, while decreased ACL_{21-35} values between 10-5.5 cal ky BP may result from the prevalence of submerged aquatic plants (Fig. 4b). The P-aqueous (P_{aq}) ratio can help differentiate between submerged plants that tend to have medium-chain-length *n*-alkanes and terrestrial plants that tend to have longer chain lengths (Ficken et al., 2000). This ratio is calculated as $(C_{23} + C_{25})/(C_{23} + C_{25}+C_{29}+C_{31})$. When the P_{aq} ratio is closer to 1, these values indicate a

15 greater percentage of submerged plants, and when the value is closer to 0, these numbers pertain to a greater percentage of terrestrial vegetation. The Paru Co P_{aq} ratio (Fig. 4c) rapidly fluctuates in the oldest section of the core, suggesting quick transitions between terrestrial and aqueous vegetation as the dominant source of *n*-alkanes to the lake. The ACL_{21-35} and P_{aq} are highly negatively correlated (r = -0.89; p-value $4.8*10^{-22}$) throughout the Paru Co core demonstrating that both ratios record similar vegetation changes during the same time periods (Fig. 4). Higher ACL ratios and lower P_{aq} values demonstrate higher

20 percentages of terrestrial plants, and vice versa.

Fluctuations in lake levels (Fig. 4d) can be associated with fluctuations in P_{aq}, suggesting a general relationship between higher lake levels and the prevalence of submerged plants between 10 and 5 cal ky BP. The opposite situation occurs between 5 and 1.3 cal ky BP, when a decreasing trend in lake level corresponds to diminishing P_{aq} values. ACL confirms this trend where the majority of values near 25 occur during higher lake levels (10-5 cal ky BP) and the majority of values around 27 occur from 5

25 to 1.3 cal ky BP. These high lake levels (Fig. 4d) are consistent with wet conditions from a more intense ISM prevailing until ~ 6 cal ky BP, as evidenced by dD wax and pollen records (Figs. 3, 4 and 5).

After 5.2 cal ky BP, lake levels decreased, suggesting diminished ISM rainfall, reduced clastic deposition, leading to an invasion of the littoral zone on the core site and an increase in sand deposition (Bird et al., 2014). The fluctuations in both ACL and P_{aq} are consistent with these lake level changes (Figs. 4 and 5). The mid to late Holocene changes in the lake levels

30 and vegetation respond to decreased summer radiation and associated ISM precipitation (Berger and Loutre, 1991).

The decline in forest vegetation and the rise in steppe vegetation from 5-4 cal ky BP seems to coincide with an increased human presence on the TP. Grazing indicators (increases in *Rumex*, *Sanguisorba,* and Apiaceae pollen), imply a human influence on the environment since approximately 3.4 cal ky BP near the south-eastern TP Lake Naleng (Kramer et al., 2010a), in the region of Paru Co. Humans slashed and burned the forests near Lhasa to open lands through fire over the past 4600 years (Miehe et al., 2006). Other studies also suggest links between fire activity and forest clearance in the southern and south-eastern TP during the late Holocene (Kaiser et al., 2009a; Kaiser et al.,2009b). Although evidence exists that humans altered TP vegetation through burning in the late Holocene, the extent of human-related vegetation change across the TP is still unknown. The absence of anthropogenic FeSts in Paru Co sediments indicates that human and associated pastoralism were not present in the local area. In Paru Co, the only FeSts above the MDL were sitosterol and sitostanol (Supplement S7). Sitosterol can derive from terrestrial vegetation, and the presence of its derivative molecule sitostanol can indicate the microbial reduction of sitosterol in the stomach of ruminant animals (Vane et al., 2010), as well as sitosterol hydrogenation in sediments (Martins et al., 2007). Sitostanol and sitosterol highly correlate with each other throughout the Paru Co core ($r = 0.94$, p-value $3.79*10^{-8}$). The fact that sitosterol and sitostanol were the only FeSts detected in Paru Co suggests the absence of ruminant animals that would also deposit other FeSts, and we consider vegetation and hydrogenation in sediments as the main sources of Paru Co FeSts. Due to the absence of other human/animal indicators, we are inclined to describe the variations in fire regimes and vegetation as primarily climate-driven signals.

Isotopic and pollen information from surrounding lakes supports the climatic variation from a warm-humid early Holocene to a cold-dry mid to late Holocene and also ascribe these climate changes to the ISM (Kramer et al., 2010a, 2010b; Ma et al., 2014; Zhu et al., 2010). Pollen assemblages from two transects of lakes (east-west and north-south) across the TP indicate sparse vegetation with low pollen concentrations characterized by *Artemisia*/Cyperaceae alpine steppe (Li et al., 2016). Lake Naleng, also located on the south-eastern TP, records changes that are similar to Paru Co paleoreconstructions (Kramer et al., 2010a). From 10.7 to 4.4 cal ky BP, open *Abies–Betula* forests reflect intense summer monsoon and an upward treeline shift. Temperature range reconstructions demonstrate climate 2-3 °C warmer than present and treeline position 400–600 m higher than today. However, within this warm period, the climate had a sudden, intense change between 8.1 and 7.2 cal ky BP with temperatures 1-2 °C below early and mid-Holocene levels and forests retreating downslope (Kramer et al., 2010a). Multiple pollen studies using compilations of Chenopodiaceae, Asteraceae, Cistaceae, Tamaricaceae, and Pottiaceae confirm the severe early Holocene cold events at 8.7–8.3 and 7.4 cal ky BP (Miao et al., 2015; Mischke and Zhang, 2010). During the mid-Holocene (7.3–4.4 cal ky BP), dense temperate steppe vegetation dominated the TP (Li et al., 2016; Zhao et al., 2011). Tree pollen (primarily *Picea*) peaks during the mid-Holocene at 6.5 cal ky BP, and then decreases until 2 cal ky BP (Zhao et al., 2011). During this same time period, Cyperaceae becomes the dominant regional steppe vegetation, and altitudinal vegetation belts shifted downslope in response to reduced temperatures (Li et al., 2016). These alpine steppes contain arid vegetation elements (including Cyperaceae, Poaceae (grass family), Amaranthaceae (pigweed and amaranths), and characteristic high-alpine herb families) between 4.4-0 cal ky BP (Herzschuh et al., 2006; Tang et al., 2000). Lake records from Nam Co and Taro

Co, located in the same vegetation zone as Paru Co, suggest a weakening in the ISM and the increased influence of the westerlies from 5.6 to 0.9 cal ky BP (Bird et al., 2014; Li et al., 2011; Ma et al., 2014). This synthesis on changes in Holocene vegetation suggests that variations of monsoonal precipitation and insolation-driven temperature are the predominant driving forces for changes in alpine vegetation in the central TP (Li et al., 2016).

5.4 Atmospheric transport

The TP is ringed by high mountains that create natural barriers that block the transport of smoke aerosols to the TP from the south, west, and northwest (You et al., 2016a). However, the ISM system may help transport both mineral and organic aerosols over the mountain ridges and into the TP during the summer monsoon months when winds rush from the south across the Himalayas. The ISM is the main source of precipitation across much of the southern TP, where this rainfall provides moisture for plant growth. The strength of the ISM over millennial timescales is driven by solar radiation, where increased insolation results in the ISM moisture moving northward across the TP. Climatic records from areas surrounding the TP demonstrate that the Pleistocene-Holocene transition was characterised by increasing temperatures until approximately 8.2 cal ky BP, when a sudden cooling occurred (Mischke et al., 2016). The ISM was more intense than current levels between ca 10-6 cal ky BP due to increased insolation, and reached a maximum in the south-eastern TP at 8 cal ky BP (Tang et al., 2000).

The mid-Holocene (~6 cal ky BP) had higher average summer sea surface temperatures (SST) and a stronger summer monsoon than during the present, resulting in a warm and wet climate (Wei et al., 2007; Zhao et al., 2011). This timing is consistent with paleo-monsoon records from southern China and with the idea that the interactions between summer insolation and other large-scale boundary conditions, including SST and sea-level change, control regional climate (Zhao et al., 2011). A drying trend during the past 6 cal ky is documented in many records from the northern subtropics and tropics (Liu and Feng, 2012). The cooling trend after the Holocene Climatic Optimum (6.5-4.7 cal ky BP) correlates with decreasing solar insolation (Zhao et al., 2011), resulting in the decreasing strength of the Asian monsoon systems and in a drier climate across much of the TP. Decreased solar insolation resulted in a dramatic drying at ~ 4.2 cal ky BP, directly or indirectly leading to the observed collapses of many Chinese Neolithic cultures (Liu and Feng, 2012; Wang et al., 2005). During the past 750 years, precipitation changes have influenced fire-regimes and vegetation shifts in the Altai, where ecosystems are highly sensitive to occasional decadal-scale drought events which, in the future, may trigger unprecedented environmental reorganization under global-warming conditions (Eichler et al., 2011).

This monsoonal history may affect the transport of fire products to Paru Co. The difference between the Paru Co MAs and PAHs records may be influenced not only by the burning temperatures that produce the different products (Section 5.1), but may also reflect changing atmospheric transport. MAs peak during the ISM maximum at Paru Co between 10 and 7 cal ky BP, which may reflect the long range transport of these fire aerosols associated with biomass burning on regional scales (Fig. 4). MAs are generally considered as regional signals due to their ability to be transported longer distances than the more local

PAHs, where this early Holocene levoglucosan peak may reflect either increased fire activity and/or changes in atmospheric transport. We may hypothesise that high levoglucosan concentrations during the early Holocene in Paru Co reflect the interplay between increasing influence of the ISM in the early Holocene resulting in wetter conditions and increase biomass on the southern TP (An et al., 2012) as well as increased Early Holocene winter monsoons causing a cold and dry climate on the north-eastern TP that is cited as a main driver for fire activity during this time period (Miao et al., 2017). Major transport to Paru Co could have come from the south via the ISM but, to best of our knowledge, no studies encompassing Holocene fire history exist from the possible southern source areas.

Even though modern transport is not indicative of atmospheric circulation in the early Holocene, recent studies can depict the distribution of air masses affecting the southern Tibetan Plateau under current monsoon conditions, and demonstrate the geographic reach of possible source areas. Modern transport patterns demonstrate that air masses over Ranwu, a sampling site in the Tibetan Plateau, 450 km east of Paru Co (Wang et al., 2016), mostly arrive from Bangladesh and the Indo-Gangetic Plain during both the winter (64.3%) and spring (70.2%) seasons (Wang et al., 2016). The remaining fraction of air masses in winter (35.7%) come from the Middle East, Afghanistan, Pakistan, and northwest India, while the spring air masses largely derive from northwest India (26.3%). Winter air masses over Beiluhe, a sampling site 600 km north of Paru Co, in the central Tibetan Plateau, come mostly from the southern slope of the Himalayas (79.6%) with the remaining air masses originating in the Middle East and Central Asia (20.4%). However, spring air masses largely originate from north-western China (45.9%), followed by Central Asia (32.4%) as well as the southern slope of the Himalayas (21.6%). The Paru Co levoglucosan record therefore encompasses possible source regions that may extend beyond the TP.

Although PAHs are more of a local fire indicator than levoglucosan concentrations, PAHs are also affected by changes in atmospheric transport and associated precipitation. PAHs peak during periods of less intense ISM precipitation, as indicated by Paru Co lithics % in the periods 10.5-10.1, 7-5.8, and 5.2-3.2 cal ky B (Fig. 4), as more intense rainfall results in greater lithic deposition (Bird et al., 2014). During these drier phases aridity could have increased regional fire activity (Section 5.1). However, this relationship between aridity and fire is not constant for the late Holocene Paru Co record as the increasing PAHs signal from 3 to 1.3 cal ky BP coincides with increasing lithic abundances that may be related to more ISM precipitation. Therefore, the 3-1.3 cal ky BP increasing PAHs could be related to a fire signal transported by ISM precipitation. Rainfall occurring together with or soon after with fire events scavenges PAHs particles from the atmosphere and increases deposition (Denis et al., 2012).

The late-Holocene PAHs fire signal in Paru Co is consistent with charcoal records demonstrating an increasing fire trend in the eastern monsoonal region of China during this same time period (Xue et al., 2018). The increasing fires in Paru Co and surrounding areas are synchronous with the general change in the regional fire pattern during the late Holocene, coincident with increases in population and crop areas (Marlon et al., 2013). Although human FeSts were absent in Paru Co, FeSts are a very local indicator of the presence of humans, and anthropogenic activity could still influence fire records across regional

scales. For example, Miao et al. (2017) link NE Tibet Bronze Age sites and associated human activity to increasing charcoal concentrations from 3.6 cal ky BP to the present.

6 Conclusions

This study is the first multi-proxy work of paleofire activity in lacustrine sediments from the Tibetan Plateau (TP) and provides a starting point for future investigations. The combination of MAs, PAHs, FeSts, and *n*-alkanes as fire and vegetation biomarkers help reconstruct the biomass burning history of the south-eastern TP. Vegetation reconstructed from MA and *n*-alkane ratios was characterised by short-term oscillations alternating between conifer and grass/steppe communities influenced by a long-term pattern of orbital-induced insolation changes. The apparent absence of human impact indicators as determined by the lack of human FeSts above the MDL excludes local anthropogenic influence on fire and vegetation changes.

The fire and vegetation records in Paru Co are instead primarily driven by climatic factors as follows:

- **Early Holocene: 10.7-7.5 cal ky BP.** The period was characterised by an increasingly warm climate followed by an intensification phase of the ISM until the mid-Holocene. These conditions may have favoured vegetation growth. Early Holocene pollen records indicate meadows as the prevalent regional vegetation in the surroundings of Paru Co, where *n*-alkane ratios depict oscillations between grass and conifer communities during much of this time period. The predominance of high molecular weight PAHs suggests high-temperature local fires during this time period. Levoglucosan also peaks during the early Holocene, suggesting that smouldering fires also occurred, although these fires may be regional rather than local. The presence of both high- and low-temperature fires is consistent with the grassland and conifer forests suggested by the *n*-alkane ratios.

- **Mid-Holocene: 7.5-3.8 cal ky BP**. The strong ISM during the early mid-Holocene increased forest vegetation near Paru Co. The peak in L/M suggests sustained fires at temperatures centred around ~300° C, which is consistent with conifer fires. The forest cover decreases beginning ~5 cal ky BP, never regaining its dominance. As the ISM decreased in strength, PAHs record intense fires, which may be due to the combination of the initial vegetation growth followed by an extended dry period. Cold and dry conditions reached their maximum at ~4.2 cal ky BP, coinciding with the expansion of local civilizations, whose eventual impact on the landscape is still unknown. However, the lack of quantifiable FeSts in the Paru Co core suggests that local populations did not live within the lake's watershed during this time period.

- **Late Holocene: 3.8-1.3 cal ky BP.** Grassy steppes dominated the vegetation near Paru Co, due to the weaker summer insolation, cooler conditions, and reduced precipitation. Although grassland dominated the region, the MAs demonstrate that relatively few smouldering fires occurred during the late Holocene. However, all combustion PAHs, including the high-temperature PAHs, demonstrate a steady increase throughout the late Holocene even though the climate and vegetation types remained stable. This PAHs trend suggests a net increase in local to regional combustion that is separate from vegetation and climate change.

Data availability. The full dataset is available in the Supplementary Information and can be accessed at the NOAA/World Data Service for Paleoclimatology archive (https://www.ncdc.noaa.gov/paleo-search/study/24410). Additional data used in this study were retrieved from Berger and Loutre (1991), Bird et al. (2014) - https://www.ncdc.noaa.gov/paleo/study/16399, Huffman et al. (2009) and Zhao et al. (2011).

5 *Competing interests*. The authors declare that they have no conflict of interest.

Acknowledgements. This work was funded as part of the Early Human Impact project, "Ideas" Specific Programme - European Research Council - Advanced Grant 2010 - Grant Agreement no. 267696, and was part of a PhD program in Environmental Sciences at Ca' Foscari University. This research was supported in part by the United States National Science Foundation (grant nos 1405072 and 1023547) and the National Natural Science Foundation of China (grant no. 41150110153). Data from
10 Zhao et al. (2011) were retrieved from the Neotoma Paleoecology Database (http://www.neotomadb.org), and the work of the data contributors and the Neotoma community is gratefully acknowledged. We are thankful to all the colleagues who helped in the lab and all the research team. We thank Aaron Diefendorf, Laura Strickland, the three anonymous referees and Dr. Toney for their helpful suggestions for improving the work. Any use of trade, firm, or product names is for descriptive purposes only and does not imply endorsement by the U.S. Government.

15 **References**

Abdel-Shafy, H. I. and Mansour, M. S. M.: A review on polycyclic aromatic hydrocarbons : Source , environmental impact , effect on human health and remediation, Egypt. J. Pet., 25(1), 107–123, doi:10.1016/j.ejpe.2015.03.011, 2016.

Aichner, B., Herzschuh, U. and Wilkes, H.: Influence of aquatic macrophytes on the stable carbon isotopic signatures of sedimentary organic matter in lakes on the Tibetan Plateau, Org. Geochem., 41(7), 706–718,
20 doi:10.1016/j.orggeochem.2010.02.002, 2010.

An, B. E. Y., Opp, R. I. F. B., Brajano, T. E. A. A., Haky, D. A. C. and Hillrud, S. T. N. C.: Source apportionment of polycyclic aromatic hydrocarbons (PAHs) into Central Park Lake , New York City , over a century of deposition, Environ. Toxicol. Chem., 33(5), 985–992, doi:10.1002/etc.2507, 2014.

An, Z., Colman, S. M., Zhou, W., Li, X., Brown, E. T., Jull, A. J. T., Liu, W., Jin, Z., Liu, X., Cheng, P., Liu, Y., Ai, L., Li,
25 X., Liu, X. and Xu, X.: Interplay between the Westerlies and Asian monsoon recorded in Lake Qinghai sediments since 32 ka, Sci. Rep., 2(619), 1–7, doi:10.1038/srep00619, 2012.

Argiriadis, E., Rada, E. C., Vecchiato, M., Zambon, S., Ionescu, G., Schiavon, M., Ragazzi, M. and Gambaro, A.: Assessing the influence of local sources on POPs in atmospheric depositions and sediments near Trento (Italy), Atmos. Environ., 98, 32–40, doi:10.1016/j.atmosenv.2014.08.035, 2014.

30 ATSDR, A. for T. S. and D.: Toxicological profile for Polycyclic Aromatic Hydrocarbons (PAHs). [online] Available from: https://www.atsdr.cdc.gov/toxprofiles/tp.asp?id=122&tid=25#bookmark12, 1995.

Battistel, D., Piazza, R., Argiriadis, E., Marchiori, E., Radaelli, M. and Barbante, C.: GC-MS method for determining faecal sterols as biomarkers of human and pastoral animal presence in freshwater sediments, Anal. Bioanal. Chem., 407(28), 8505–8514, doi:10.1007/s00216-015-8998-2, 2015.

Battistel, D., Argiriadis, E., Kehrwald, N., Spigariol, M., Russell, J. M. and Barbante, C.: Fire and human record at Lake Victoria , East Africa , during the Early Iron Age : Did humans or climate cause massive ecosystem changes during the Early Iron Age in East Africa?, The Holocene, doi:10.1177/0959683616678466, 2016.

Berger, A. and Loutre, M. F.: Insolation values for the climate of the last 10 million years, Quat. Sci. Rev., 10(4), 297–317, doi:10.1016/0277-3791(91)90033-Q, 1991.

Bird, B. W., Polisar, P. J., Lei, Y., Thompson, L. G., Yao, T., Finney, B. P., Bain, D. J., Pompeani, D. P. and Steinman, B. A.: A Tibetan lake sediment record of Holocene Indian summer monsoon variability, Earth Planet. Sci. Lett., 399, 92–102, doi:10.1016/j.epsl.2014.05.017, 2014.

Bird, B. W., Lei, Y., Perello, M., Polissar, P. J., Yao, T., Finney, B., Bain, D., Pompeani, D. and Thompson, L. G.: Late-Holocene Indian summer monsoon variability revealed from a 3300-year-long lake sediment record from Nirpa Co, southeastern Tibet, The Holocene, 27(4), 541–552, doi:10.1177/0959683616670220, 2017.

Bowman, D. M. J. S., Balch, J. K., Artaxo, P., Bond, W. J., Carlson, J. M., Cochrane, M. a., D'Antonio, C. M., Defries, R. S., Doyle, J. C., Harrison, S. P., Johnston, F. H., Keeley, J. E., Krawchuk, M. a., Kull, C. a., Marston, J. B., Moritz, M. a., Prentice, I. C., Roos, C. I., Scott, a. C., Swetnam, T. W., van der Werf, G. R. and Pyne, S. J.: Fire in the Earth system., Science (80-.)., 324(5926), 481–4, doi:10.1126/science.1163886, 2009.

Bray, E. . and Evans, E. .: Distribution of n-paraffins as a clue to recognition of source beds, Geochim. Cosmochim. Acta, 22(1), 2–15, doi:10.1016/0016-7037(61)90069-2, 1961.

Bull, I. D., Matthew J. Lockheart, Mohamed M. Elhmmali, David J. Roberts and Richard P. Evershed: The Origin of Faeces by Means of Biomarker Detection, Environ. Int., 27, 647–654, doi:S0160-4120(01)00124-6, 2002.

Bush, R. T. and McInerney, F. A.: Leaf wax n-alkane distributions in and across modern plants: Implications for paleoecology and chemotaxonomy, Geochim. Cosmochim. Acta, 117, 161–179, doi:10.1016/j.gca.2013.04.016, 2013.

Cai, Q., Mo, C., Wu, Q., Katsoyiannis, A. and Zeng, Q.: The status of soil contamination by semivolatile organic chemicals (SVOCs) in China: A review, Sci. Total Environ., 389, 209–224, doi:10.1016/j.scitotenv.2007.08.026, 2008.

Carr, A. S., Boom, A., Grimes, H. L., Chase, B. M., Meadows, M. E. and Harris, A.: Leaf wax n-alkane distributions in arid zone South African flora: Environmental controls, chemotaxonomy and palaeoecological implications, Org. Geochem., 67, 72–84, doi:10.1016/j.orggeochem.2013.12.004, 2014.

Cui, J., Huang, J. and Xie, S.: Characterstics of seasonal variations of leaf n-alkanes and n-alkenes in modern higher plants in Qingjiang, Hubei Province, China, Chinese Sci. Bull., 53(17), 2659–2664, doi:10.1007/s11434-008-0194-8, 2008.

D'Anjou, R. M., Bradley, R. S., Balascio, N. L. and Finkelstein, D. B.: Climate impacts on human settlement and agricultural activities in northern Norway revealed through sediment biogeochemistry., Proc. Natl. Acad. Sci. U. S. A., 109(50), 20332–20337, doi:10.1073/pnas.1212730109, 2012.

Dallmeyer, A., Claussen, M., Herzschuh, U. and Fischer, N.: Holocene vegetation and biomass changes on the Tibetan Plateau - A model-pollen data comparison, Clim. Past, 7(3), 881–901, doi:10.5194/cp-7-881-2011, 2011.

Daly, G. L., Lei, Y. D., Castillo, L. E., Muir, D. C. G. and Wania, F.: Polycyclic aromatic hydrocarbons in Costa Rican air and soil: A tropical/temperate comparison, Atmos. Environ., 41(34), 7339–7350, doi:10.1016/j.atmosenv.2007.05.014, 2007.

5   Daughton, C. G.: Real-time estimation of small-area populations with human biomarkers in sewage., Sci. Total Environ., 414, 6–21, doi:10.1016/j.scitotenv.2011.11.015, 2012.

Dietze, E., Wünnemann, B., Hartmann, K., Diekmann, B., Jin, H., Stauch, G., Yang, S. and Lehmkuhl, F.: Early to mid-Holocene lake high-stand sediments at Lake Donggi Cona, northeastern Tibetan Plateau, China, Quat. Res. (United States), 79(3), 325–336, doi:10.1016/j.yqres.2012.12.008, 2013.

10   Dong, H., Jiang, H., Yu, B., Liu, X. and Zhang, C.: Impacts of environmental change and human activity on microbial ecosystems on the Tibetan Plateau, NW China, GSA Today, 20(6), 4–10, doi:10.1130/GSATG75A.1, 2010.

Douglas, P. M. J., Pagani, M., Brenner, M., Hodell, D. A. and Curtis, J. H.: Aridity and vegetation composition are important determinants of leaf-wax dD values in southeastern Mexico and Central America, Geochim. Cosmochim. Acta, 97, 24–45, doi:10.1016/j.gca.2012.09.005, 2012.

15   Dubois, N. and Jacob, J.: Molecular Biomarkers of Anthropic Impacts in Natural Archives: A Review, Front. Ecol. Evol., 4(August), 1–16, doi:10.3389/fevo.2016.00092, 2016.

Eichler, A., Tinner, W., Brütsch, S., Olivier, S., Papina, T. and Schwikowski, M.: An ice-core based history of Siberian forest fires since AD 1250, Quat. Sci. Rev., 30(9–10), 1027–1034, doi:10.1016/j.quascirev.2011.02.007, 2011.

Fabbri, D., Torri, C., Simoneit, B. R. T., Marynowski, L., Rushdi, A. I. and Fabiańska, M. J.: Levoglucosan and other cellulose
20   and lignin markers in emissions from burning of Miocene lignites, Atmos. Environ., 43(14), 2286–2295, doi:10.1016/j.atmosenv.2009.01.030, 2009.

Ficken, K. J., Street-Perrott, F. A., Perrott, R. A., Swain, D. L., Olago, D. O. and Eglinton, G.: Glacial/interglacial variations in carbon cycling revealed by molecular and isotope stratigraphy of Lake Nkunga, Mt. Kenya, East Africa, Org. Geochem., 29(5–7), 1701–1719, doi:10.1016/S0146-6380(98)00109-0, 1998.

25   Ficken, K. J., Li, B., Swain, D. L. and Eglinton, G.: An n-alkane proxy for the sedimentary input of submerged/floating freshwater aquatic macrophytes, Org. Geochem., 31(7–8), 745–749, doi:10.1016/S0146-6380(00)00081-4, 2000.

Gabrieli, J., Vallelonga, P., Cozzi, G., Gabrielli, P., Gambaro, A., Sigl, M., Decet, F., Schwikowski, M., Gäggeler, H., Boutron, C., Cescon, P. and Barbante, C.: Post 17th-century changes of european pah emissions recorded in high-altitude alpine snow and ice, Environ. Sci. Technol., 44(9), 3260–3266, doi:10.1021/es903365s, 2010.

30   García-alix, A., Jim, F. J., Toney, J. L., Jiménez-moreno, G., Ramos-román, M. J., Anderson, R. S., Ruano, P., Queralt, I., Huertas, A. D. and Kuroda, J.: Alpine bogs of southern Spain show human-induced environmental change superimposed on long-term natural variations, Sci. Rep., 7(7439), 1–12, doi:10.1038/s41598-017-07854-w, 2017.

Gregoris, E., Argiriadis, E., Vecchiato, M., Zambon, S., De Pieri, S., Donateo, A., Contini, D., Piazza, R., Barbante, C. and Gambaro, A.: Gas-particle distributions, sources and health effects of polycyclic aromatic hydrocarbons (PAHs),

polychlorinated biphenyls (PCBs) and polychlorinated naphthalenes (PCNs) in Venice aerosols, Sci. Total Environ., 476–477, 393–405, doi:10.1016/j.scitotenv.2014.01.036, 2014.

Grimalt, J. and Albaigés, J.: Sources and occurrence of C12-C22n-alkane distributions with even carbon-number preference in sedimentary environments, Geochim. Cosmochim. Acta, 51(6), 1379–1384, doi:10.1016/0016-7037(87)90322-X, 1987.

5   Han, J. and Calvin, M.: Hydrocarbon distribution of algae and bacteria, and microbiological activity in sediments., Proc. Natl. Acad. Sci. U. S. A., 64(Table 1), 436–443, doi:10.1073/pnas.64.2.436, 1969.

Haritash, A. K. and Kaushik, C. P.: Biodegradation aspects of Polycyclic Aromatic Hydrocarbons (PAHs): A review, J. Hazard. Mater., 169(1–3), 1–15, doi:10.1016/j.jhazmat.2009.03.137, 2009.

Herrmann, M., Lu, X., Berking, J., Schütt, B., Yao, T. and Mosbrugger, V.: Reconstructing Holocene vegetation and climate
10 history of Nam Co area (Tibet), using pollen and other palynomorphs, Quat. Int., 218(1–2), 45–57, doi:10.1016/j.quaint.2009.05.007, 2010.

Herzschuh, U., Winter, K., Wünnemann, B. and Li, S.: A general cooling trend on the central Tibetan Plateau throughout the Holocene recorded by the Lake Zigetang pollen spectra, Quat. Int., 154–155, 113–121, doi:10.1016/j.quaint.2006.02.005, 2006.

15 Huffman G.J., Adler R.F., Bolvin D.T., N. E. J.: The TRMM Multi-Satellite Precipitation Analysis (TMPA)., in Satellite Rainfall Applications for Surface Hydrology, edited by H. F. Gebremichael M., 2009.

Hughes, I. G. and Hase, T. P. A.: Measurements and their Uncertainties, 1st ed., Oxford University Press Inc., New York., 2010.

IPCC: Summary for Policymakers, edited by R. K. P. and L. A. M. (eds. . Core Writing Team, Geneva., 2014.

20 Jiang, C., Alexander, R., Kagi, R. I. and Murray, A. P.: Polycyclic aromatic hydrocarbons in ancient sediments and their relationships to palaeoclimate, Org. Geochem., 29(5–7–7 pt 2), 1721–1735, doi:10.1016/S0146-6380(98)00083-7, 1998.

Johnsen, A. R., Wick, L. Y. and Harms, H.: Principles of microbial PAH-degradation in soil, Environ. Pollut., 133(1), 71–84, doi:10.1016/j.envpol.2004.04.015, 2005.

Kaiser, K., Opgenoorth, L., Schoch, W. H. and Miehe, G.: Charcoal and fossil wood from palaeosols, sediments and artificial
25 structures indicating Late Holocene woodland decline in southern Tibet (China), Quat. Sci. Rev., 28(15–16), 1539–1554, doi:10.1016/j.quascirev.2009.02.016, 2009a.

Kaiser, K., Lai, Z., Schneider, B., Reudenbach, C., Miehe, G. and Brückner, H.: Stratigraphy and palaeoenvironmental implications of Pleistocene and Holocene aeolian sediments in the Lhasa area, southern Tibet (China), Palaeogeogr. Palaeoclimatol. Palaeoecol., 271(3–4), 329–342, doi:10.1016/j.palaeo.2008.11.004, 2009b.

30 Kaspari, S. D., Schwikowski, M., Gysel, M., Flanner, M. G., Kang, S., Hou, S. and Mayewski, P. A.: Recent increase in black carbon concentrations from a Mt. Everest ice core spanning 1860-2000 AD, Geophys. Res. Lett., 38(4), 11–16, doi:10.1029/2010GL046096, 2011.

Kehrwald, N.: Decadal-scale changes in East African fire activity for the past 4000 years, Quat. Int., 279–280(2012), 239, doi:10.1016/j.quaint.2012.08.545, 2012.

Kim, K.-H., Jahan, S. A., Kabir, E. and Brown, R. J. C.: A review of airborne polycyclic aromatic hydrocarbons (PAHs) and their human health effects., Environ. Int., 60, 71–80, doi:10.1016/j.envint.2013.07.019, 2013.

Kirchgeorg, T.: Specific molecular markers in lake sediment cores for biomass burning reconstruction during the Holocene, , 1–90, 2015.

Kirchgeorg, T., Schüpbach, S., Kehrwald, N., McWethy, D. B. and Barbante, C.: Method for the determination of specific molecular markers of biomass burning in lake sediments, Org. Geochem., 71, 1–6, doi:10.1016/j.orggeochem.2014.02.014, 2014.

Kramer, A., Herzschuh, U., Mischke, S. and Zhang, C.: Holocene treeline shifts and monsoon variability in the Hengduan Mountains (southeastern Tibetan Plateau), implications from palynological investigations, Palaeogeogr. Palaeoclimatol. Palaeoecol., 286, 23–41, doi:10.1016/j.palaeo.2009.12.001, 2010a.

Kramer, A., Herzschuh, U., Mischke, S. and Zhang, C.: Late glacial vegetation and climate oscillations on the southeastern Tibetan Plateau inferred from the Lake Naleng pollen profile, Quat. Res., 73, 324–335, doi:10.1016/j.yqres.2009.12.003, 2010b.

Kuo, L. J., Louchouarn, P. and Herbert, B. E.: Influence of combustion conditions on yields of solvent-extractable anhydrosugars and lignin phenols in chars: Implications for characterizations of biomass combustion residues, Chemosphere, 85(5), 797–805, doi:10.1016/j.chemosphere.2011.06.074, 2011.

Li, Q., Lu, H., Zhu, L., Wu, N., Wang, J. and Lu, X.: Pollen-inferred climate changes and vertical shifts of alpine vegetation belts on the northern slope of the Nyainqentanglha Mountains (central Tibetan Plateau) since 8.4 kyr BP, The Holocene, 21(6), 939–950, doi:10.1177/0959683611400218, 2011.

Li, Q., Lu, H., Shen, C., Zhao, Y. and Ge, Q.: Vegetation successions in response to Holocene climate changes in the central Tibetan Plateau, J. Arid Environ., 125, 136–144, doi:10.1016/j.jaridenv.2015.07.010, 2016.

Lima, A. L. C., Farrington, J. W. and Reddy, C. M.: Combustion-Derived Polycyclic Aromatic Hydrocarbons in the Environment—A Review, Environ. Forensics, 6(2), 109–131, doi:10.1080/15275920590952739, 2005.

Liping Zhu, Yanhong Wu, Junbo Wang, Xiao Lin, Jianting Ju, Manping Xie, Minghui Li, Mausbacher, R., Schwalb, A. and Daut, G.: Environmental changes since 8.4 ka reflected in the lacustrine core sediments from Nam Co, central Tibetan Plateau, China, The Holocene, 18, 831–839, doi:10.1177/0959683608091801, 2008.

Liu, F. and Feng, Z.: A dramatic climatic transition at ~4000 cal. yr BP and its cultural responses in Chinese cultural domains, The Holocene, 22(10), 1181–1197, doi:10.1177/0959683612441839, 2012.

Liu, K. B., Yao, Z. J. and Thompson, L. G.: A pollen record of Holocene climatic changes from the Dunde ice cap, Qinghai-Tibetan Plateau, Geology, 26(2), 135–138, doi:10.1130/0091-7613(1998)026<0135, 1998.

Liu, X., Dong, H., Rech, J. A., Matsumoto, R., Bo, Y. and Yongbo, W.: Evolution of Chaka Salt Lake in NW China in response to climatic change during the Latest Pleistocene-Holocene, Quat. Sci. Rev., 27(7–8), 867–879, doi:10.1016/j.quascirev.2007.12.006, 2008.

Liu, X., Dong, H., Yang, X., Herzschuh, U., Zhang, E., Stuut, J. B. W. and Wang, Y.: Late Holocene forcing of the Asian

winter and summer monsoon as evidenced by proxy records from the northern Qinghai-Tibetan Plateau, Earth Planet. Sci. Lett., 280(1–4), 276–284, doi:10.1016/j.epsl.2009.01.041, 2009.

Lu, H., Wu, N., Liu, K. biu, Zhu, L., Yang, X., Yao, T., Wang, L., Li, Q., Liu, X., Shen, C., Li, X., Tong, G. and Jiang, H.: Modern pollen distributions in Qinghai-Tibetan Plateau and the development of transfer functions for reconstructing Holocene environmental changes, Quat. Sci. Rev., 30(7–8), 947–966, doi:10.1016/j.quascirev.2011.01.008, 2011.

Ma, L., Chu, S., Cheng, H., Wang, X., Liu, X. and Xu, X.: Polycyclic aromatic hydrocarbons contamination in subsoil from outskirts of Beijing, People's Republic of China, Geoderma, 129(3–4), 200–210, doi:10.1016/j.geoderma.2004.11.026, 2005.

Ma, Q., Zhu, L., L, X., Guo, Y., Ju, J., Wang, J., Wang, Y. and Tang, L.: Pollen-inferred Holocene vegetation and climate histories in Taro Co, southwestern Tibetan Plateau, Chinese Sci. Bull., 59(31), 4101–4114, doi:10.1007/s11434-014-0505-1, 2014.

Maliszewska-Kordybach, B., Smreczak, B. and Klimkowicz-Pawlas, A.: Concentrations, sources, and spatial distribution of individual polycyclic aromatic hydrocarbons (PAHs) in agricultural soils in the Eastern part of the EU: Poland as a case study, Sci. Total Environ., 407(12), 3746–3753, doi:10.1016/j.scitotenv.2009.01.010, 2009.

Marlon, J. R., Bartlein, P. J., Daniau, A. L., Harrison, S. P., Maezumi, S. Y., Power, M. J., Tinner, W. and Vanniére, B.: Global biomass burning: A synthesis and review of Holocene paleofire records and their controls, Quat. Sci. Rev., 65, 5–25, doi:10.1016/j.quascirev.2012.11.029, 2013.

Martino, M.: Sviluppo di un metodo per la determinazione di biomarker in campioni di torba, Ca' Foscari University of Venice. [online] Available from: http://dspace.unive.it/handle/10579/7916?show=full, 2016.

Martins, C. D. C., Fillmann, G. and Montone, R. C.: Natural and anthropogenic sterols inputs in surface sediments of Patos Lagoon, Brazil, J. Braz. Chem. Soc., 18(1), 106–115, doi:10.1590/S0103-50532007000100012, 2007.

Matsubara Pereira, F.: Paleofire activity reconstruction in the Tibetan Plateau, Università Ca' Foscari Venezia. [online] Available from: http://dspace.unive.it/handle/10579/10154?show=full, 2017.

McGrath, T. E., Chan, W. G. and Hajaligol, R.: Low temperature mechanism for the formation of polycyclic aromatic hydrocarbons from the pyrolysis of cellulose, J. Anal. Appl. Pyrolysis, 66, 51–70, 2003.

Medeiros, P. M. and Simoneit, B. R. T.: Source Profiles of Organic combustion of Green Vegetation from tempate Climate Forest, Environ. Sci. Technol., 42(22), 8310–8317, 2008.

Menounos, B.: The water content of lake sediments and its relationship to other physical parameters: an alpine case study, The Holocene, 7(2), 207–212, doi:10.1177/095968369700700208, 1997.

Meyers, P. A. and Ishiwatari, R.: Lacustrine organic geochemistry—an overview of indicators of organic matter sources and diagenesis in lake sediments, Org. Geochem., 20(7), 867–900, doi:10.1016/0146-6380(93)90100-P, 1993.

Miao, Y., Jin, H., Liu, B., Herrmann, M., Sun, Z. and Wang, Y.: Holocene climate change on the northeastern Tibetan Plateau inferred from mountain-slope pollen and non-pollen palynomorphs, Rev. Palaeobot. Palynol., 221, 22–31, doi:10.1016/j.revpalbo.2015.05.006, 2015.

Miao, Y., Zhang, D., Cai, X., Li, F., Jin, H., Wang, Y. and Liu, B.: Holocene fire on the northeast Tibetan Plateau in relation

to climate change and human activity, Quat. Int., 443, 124–131, doi:10.1016/j.quaint.2016.05.029, 2017.

Miehe, G., Miehe, S., Schlütz, F., Kaiser, K. and Duo, L.: Palaeoecological and experimental evidence of former forests and woodlands in the treeless desert pastures of Southern Tibet (Lhasa, A.R. Xizang, China), Palaeogeogr. Palaeoclimatol. Palaeoecol., 242(1–2), 54–67, doi:10.1016/j.palaeo.2006.05.010, 2006.

5 Ming, J., Cachier, H., Xiao, C., Qin, D., Kang, S., Hou, S. and Xu, J.: Black carbon record based on a shallow Himalayan ice core and its climatic implications, Atmos. Chem. Phys., 8(5), 1343–1352, doi:10.5194/acp-8-1343-2008, 2008.

Mischke, S. and Zhang, C.: Holocene cold events on the Tibetan Plateau, Glob. Planet. Change, 72(3), 155–163, doi:10.1016/j.gloplacha.2010.02.001, 2010.

Mischke, S., Lai, Z., Long, H. and Tian, F.: Holocene climate and landscape change in the northeastern Tibetan Plateau

10 foreland inferred from the Zhuyeze Lake record, The Holocene, 26(4), 643–654, doi:10.1177/0959683615612570, 2016.

Nishimura, M. and Koyama, T.: The occurrence of stanols in various living organisms and the behavior of sterols in contemporary sediments, Geochim. Cosmochim. Acta, 41(3), 379–385, doi:10.1016/0016-7037(77)90265-4, 1977.

Norwood, M. J., Louchouarn, P., Kuo, L. and Harvey, O. R.: Characterization and biodegradation of water-soluble biomarkers and organic carbon extracted from low temperature chars, Org. Geochem., 56, 111–119,

15 doi:10.1016/j.orggeochem.2012.12.008, 2013.

Opitz, S., Wünnemann, B., Aichner, B., Dietze, E., Hartmann, K., Herzschuh, U., IJmker, J., Lehmkuhl, F., Li, S., Mischke, S., Plotzki, A., Stauch, G. and Diekmann, B.: Late Glacial and Holocene development of Lake Donggi Cona, north-eastern Tibetan Plateau, inferred from sedimentological analysis, Palaeogeogr. Palaeoclimatol. Palaeoecol., 337–338, 159–176, doi:10.1016/j.palaeo.2012.04.013, 2012.

20 Page, D. S., Boehm, P. D., Douglas, G. S., Bence, A. E., Burns, W. A. and Mankiewicz, P. J.: Pyrogenic Polycyclic Aromatic Hydrocarbons in Sediments Record Past Human Activity: A Case Study in Prince William Sound, Alaska, Mar. Pollut. Bull., 38(4), 247–260, doi:10.1016/S0025-326X(98)00142-8, 1999.

Piazza, R., Gambaro, A., Argiriadis, E., Vecchiato, M., Zambon, S., Cescon, P. and Barbante, C.: Development of a method for simultaneous analysis of PCDDs, PCDFs, PCBs, PBDEs, PCNs and PAHs in Antarctic air, Anal. Bioanal. Chem., 405(2–

25 3), 917–932, doi:10.1007/s00216-012-6464-y, 2013.

Poynter, J. and Eglinton, G.: Molecular composition of three sediments from hole 717C: The Bengal fan, Proc. Ocean Drill. Program, Sci. Results, 116, 155–161, doi:10.2973/odp.proc.sr.116.151.1990, 1990.

Saini, J., Günther, F., Aichner, B., Mischke, S., Herzschuh, U., Zhang, C., Mäusbacher, R. and Gleixner, G.: Climate variability in the past ~19,000 yr in NE Tibetan Plateau inferred from biomarker and stable isotope records of Lake Donggi Cona, Quat.

30 Sci. Rev., 157, 129–140, doi:10.1016/j.quascirev.2016.12.023, 2017.

Schefuss, E., Ratmeyer, V., Stuut, J.-B. W., Jansen, J. H. F. and Sinninghe Damsté, J. S.: Carbon isotope analyses of n -alkanes in dust from the lower atmosphere over the central eastern Atlantic, Geochim. Cosmochim. Acta, 67(10), 1757–1767, doi:10.1016/S0016-7037(02)01414-X, 2003.

Schüpbach, S., Kirchgeorg, T., Colombaroli, D., Beffa, G., Radaelli, M., Kehrwald, N. M. and Barbante, C.: Combining

charcoal sediment and molecular markers to infer a Holocene fire history in the Maya Lowlands of Petén, Guatemala, Quat. Sci. Rev., 115, 123–131, doi:10.1016/j.quascirev.2015.03.004, 2015.

Severinghaus, J. P. and Brook, E. J.: Abrupt Climate Change at the End of the Last Glacial Period Inferred from Trapped Air in Polar Ice, Science (80-.)., 286(October), 930–933, doi:10.1126/science.286.5441.930, 1999.

5 Sheperd, T. and Griffiths, D. W.: The effects of stress on plant cuticular waxes, New Phytol., 171, 469–499, doi:10.1111/j.1469-8137.2006.01826.x, 2006.

Shimono, A., Zhou, H., Shen, H., Hirota, M., Ohtsuka, T. and Tang, Y.: Patterns of plant diversity at high altitudes on the Qinghai-Tibetan Plateau, J. Plant Ecol., 3(1), 1–7, doi:10.1093/jpe/rtq002, 2010.

Shugui, H., Dahe, Q., Dongqi, Z., Shichang, K., Mayewski, P. A. and Wake, C. P.: A 154 a high-resolution ammonium record
10 from the Rongbuk Glacier, north slope of Mt. Qomolangma (Everest), Tibet-Himal region, Atmos. Environ., 37(5), 721–729, doi:10.1016/S1352-2310(02)00582-4, 2003.

Simoneit, B. R. T.: Biomass burning - A review of organic tracers for smoke from incomplete combustion., 2002.

Simoneit, B. R. T., Schauer, J. J., Nolte, C. G., Oros, D. R., Elias, V. O., Fraser, M. P., Rogge, W. F. and Cass, G. R.: Levoglucosan, a tracer for cellulose in biomass burning and atmospheric particles, Atmos. Environ., 33(2), 173–182,
15 doi:10.1016/S1352-2310(98)00145-9, 1999.

Standley, L. J. and Simoneit, B. R. T.: Characterization of Extractable Plant Wax , Resin , and Thermally Matured Components in Smoke Particles from Prescribed Burns, Environ. Sci. Technol., 21, 163–169, doi:10.1021/es00156a006, 1987.

Tang, L., Shen, C., Liu, K. and Overpeck, J. T.: Changes in South Asian monsoon : New high-resolution paleoclimatic records from Tibet , China, Chinese Sci. Bull., 45(1), 87–91, 2000.

20 Vane, C. H., Kim, A. W., McGowan, S., Leng, M. J., Heaton, T. H. E., Kendrick, C. P., Coombs, P., Yang, H. and Swann, G. E. A.: Sedimentary records of sewage pollution using faecal markers in contrasting peri-urban shallow lakes., Sci. Total Environ., 409(2), 345–56, doi:10.1016/j.scitotenv.2010.09.033, 2010.

Wang, H., Zhou, X., Wan, C., Fu, H., Zhang, F. and Ren, J.: Eco-environmental degradation in the northeastern margin of the Qinghai-Tibetan Plateau and comprehensive ecological protection planning, Environ. Geol., 55(5), 1135–1147,
25 doi:10.1007/s00254-007-1061-7, 2008.

Wang, M., Xu, B., Wang, N., Cao, J., Tie, X., Wang, H., Zhu, C. and Yang, W.: Two distinct patterns of seasonal variation of airborne black carbon over Tibetan Plateau, Sci. Total Environ., 573, 1041–1052, doi:10.1016/j.scitotenv.2016.08.184, 2016.

Wang, W., Wang, Q., Li, S. and Wang, G.: Distribution and species diversity of plant communities along transect on the northeastern Tibetan Plateau, Biodivers. Conserv., 15(5), 1811–1828, doi:10.1007/s10531-004-6681-6, 2006.

30 Wang, W., Massey, S. L., Xue, M., Zhao, J., Zhang, N. and Wang, R.: Concentrations, sources and spatial distribution of polycyclic aromatic hydrocarbons in soils from Beijing, Tianjin and surrounding areas, North China, Environ. Pollut., 158, 1245–1251, doi:10.1016/j.envpol.2010.01.021, 2010.

Wang, Y., Cheng, H., Edwards, L., He, Y., Kong, X., An, Z., Wu, J., Kelly, M. J., Dykoski, C. A. and Li, X.: The Holocene Asian Monsoon: Links to Solar Changes and North Atlantic Climate, Science (80-.)., 308(5723), 854–857,

doi:10.1126/science.1106296, 2005.

Wei, G., Deng, W., Yu, K., Li, X. H., Sun, W. and Zhao, J. X.: Sea surface temperature records in the northern South China Sea from mid-Holocene coral Sr/Ca ratios, Paleoceanography, 22(3), 1–13, doi:10.1029/2006PA001270, 2007.

Wu, J., Hu, R., Yue, J., Yang, Z. and Zhang, L.: Determination of fecal sterols by gas chromatography – mass spectrometry with solid-phase extraction and injection-port derivatization, J. Chromatogr. A, 1216, 1053–1058, doi:10.1016/j.chroma.2008.12.054, 2009.

Xu, B. Q., Wang, M., Joswiak, D. R., Cao, J. J., Yao, T. D., Wu, G. J., Yang, W. and Zhao, H. B.: Deposition of anthropogenic aerosols in a southeastern Tibetan glacier, J. Geophys. Res. Atmos., 114(17), 1–8, doi:10.1029/2008JD011510, 2009.

Xue, J., Zhong, W., Li, Q., Cheng, R., You, A., Wei, Z. and Shang, S.: Holocene fi re history in eastern monsoonal region of China and its controls, Palaeogeogr. Palaeoclimatol. Palaeoecol., 496(January), 136–145, doi:10.1016/j.palaeo.2018.01.029, 2018.

Yan, D. and Wünnemann, B.: Late Quaternary water depth changes in Hala Lake, northeastern Tibetan Plateau, derived from ostracod assemblages and sediment properties in multiple sediment records, Quat. Sci. Rev., 95, 95–114, 2014.

Yang, R., Xie, T., Li, A., Yang, H., Turner, S., Wu, G. and Jing, C.: Sedimentary records of polycyclic aromatic hydrocarbons (PAHs) in remote lakes across the Tibetan Plateau, Environ. Pollut., 214, 1–7, doi:10.1016/j.envpol.2016.03.068, 2016.

Yanhong, W., Lücke, A., Zhangdong, J., Sumin, W., Schleser, G. H., Battarbee, R. W. and Weilan, X.: Holocene climate development on the central Tibetan Plateau: A sedimentary record from Cuoe Lake, Palaeogeogr. Palaeoclimatol. Palaeoecol., 234, 328–340, doi:10.1016/j.palaeo.2005.09.017, 2006.

Yao, P., Schwab, V. F., Roth, V. N., Xu, B., Yao, T. and Gleixner, G.: Levoglucosan concentrations in ice-core samples from the Tibetan Plateau determined by reverse-phase high-performance liquid chromatography-mass spectrometry, J. Glaciol., 59(216), 599–612, doi:10.3189/2013JoG12J157, 2013.

You, C., Xu, C., Xu, B., Zhao, H. and Song, L.: Levoglucosan evidence for biomass burning records over Tibetan glaciers, Environ. Pollut., 216(May), 173–181, doi:10.1016/j.envpol.2016.05.074, 2016a.

You, C., Song, L., Xu, B. and Gao, S.: Method for determination of levoglucosan in snow and ice at trace concentration levels using ultra-performance liquid chromatography coupled with triple quadrupole mass spectrometry., 2016b.

Yunker, M. B., Macdonald, R. W., Vingarzan, R., Mitchell, R. H., Goyette, D. and Sylvestre, S.: PAHs in the Fraser River basin: A critical appraisal of PAH ratios as indicators of PAH source and composition, Org. Geochem., 33(4), 489–515, doi:10.1016/S0146-6380(02)00002-5, 2002a.

Yunker, M. B., Backus, S. M., Pannatier, E. G., Je, D. S. and Macdonald, R. W.: Sources and Significance of Alkane and PAH Hydrocarbons in Canadian Arctic Rivers, Estuar. Coast. Shelf Sci., 55, 1–31, doi:10.1006/ecss.2001.0880, 2002b.

Yunker, M. B., Macdonald, R. W., Ross, P. S., Johannessen, S. C. and Dangerfield, N.: Alkane and PAH provenance and potential bioavailability in coastal marine sediments subject to a gradient of anthropogenic sources in British Columbia , Canada, Org. Geochem., 89–90, 80–116, doi:10.1016/j.orggeochem.2015.10.002, 2015.

Zakir Hossain, H. M., Sampei, Y. and Roser, B. P.: Polycyclic aromatic hydrocarbons (PAHs) in late Eocene to early

Pleistocene mudstones of the Sylhet succession, NE Bengal Basin, Bangladesh: Implications for source and paleoclimate conditions during Himalayan uplift, Org. Geochem., 56, 25–39, doi:10.1016/j.orggeochem.2012.12.001, 2013.

Zangrando, R., Barbaro, E., Zennaro, P., Rossi, S., Kehrwald, N. M., Gabrieli, J., Barbante, C. and Gambaro, A.: Molecular markers of biomass burning in Arctic aerosols, Environ. Sci. Technol., 47(15), 8565–8574, doi:10.1021/es400125r, 2013.

5   Zennaro, P., Kehrwald, N., McConnell, J. R., Schüpbach, S., Maselli, O. J., Marlon, J., Vallelonga, P., Leuenberger, D., Zangrando, R., Spolaor, A., Borrotti, M., Barbaro, E., Gambaro, A. and Barbante, C.: Fire in ice: Two millennia of boreal forest fire history from the Greenland NEEM ice core, Clim. Past, 10(5), 1905–1924, doi:10.5194/cp-10-1905-2014, 2014.

Zennaro, P., Kehrwald, N., Marlon, J., Ruddimman, W. F., Brücher, T., Agostinelli, C., Dahl-jensen, D., Zangrando, R. and Gambaro, A.: Europe on fire three thousand years ago: Arson or climate?, Geophys. Res. Lett., 5023–5033, doi:10.1002/2015GL064259, 2015.

10   Zhang, T., Claeys, M., Cachier, H., Dong, S., Wang, W., Maenhaut, W. and Liu, X.: Identification and estimation of the biomass burning contribution to Beijing aerosol using levoglucosan as a molecular marker, Atmos. Environ., 42(29), 7013–7021, doi:10.1016/j.atmosenv.2008.04.050, 2008.

Zhao, S., Tie, X., Long, X. and Cao, J.: Impacts of Himalayas on black carbon over the Tibetan Plateau during summer monsoon, Sci. Total Environ., 598, 307–318, doi:10.1016/j.scitotenv.2017.04.101, 2017.

15   Zhao, Y., Yu, Z. and Zhao, W.: Holocene vegetation and climate histories in the eastern Tibetan Plateau: Controls by insolation-driven temperature or monsoon-derived precipitation changes?, Quat. Sci. Rev., 30(9–10), 1173–1184, doi:10.1016/j.quascirev.2011.02.006, 2011.

Zhu, L., Peng, P., Xie, M., Wang, J., Frenzel, P., Wrozyna, C. and Schwalb, A.: Ostracod-based environmental reconstruction over the last 8,400 years of Nam Co Lake on the Tibetan plateau, Hydrobiologia, 648(1), 157–174, doi:10.1007/s10750-010-0149-3, 2010.
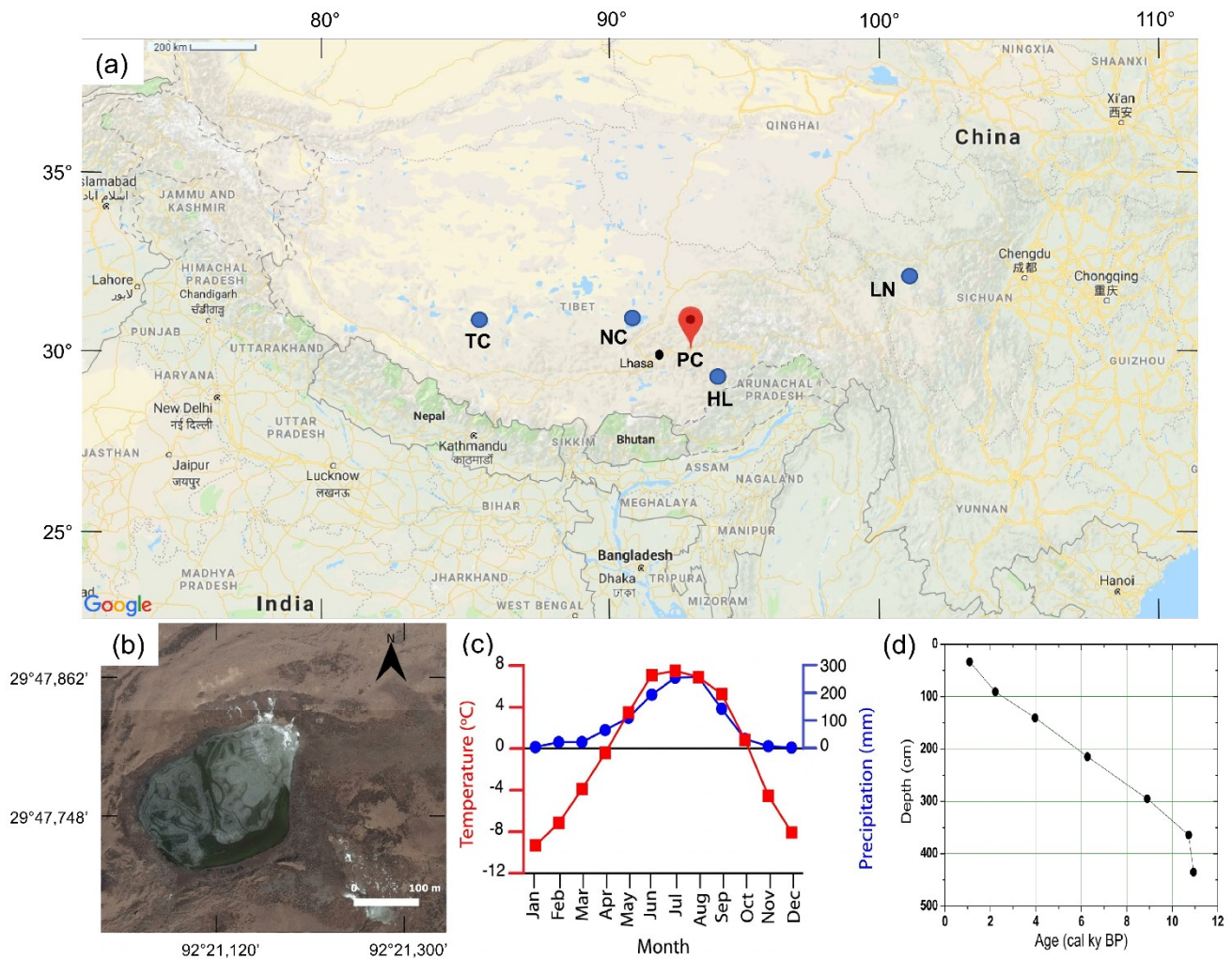
Figure 1: (a) Map of the Tibetan Plateau and surrounding territories showing the location of Paru Co (red pin) and of the other lakes mentioned in the text (blue circles): Taro Co (TC), Nam Co (NC), Hidden Lake (HL) and Lake Naleng (LN). (b) Satellite image of Paru Co. (c) Average monthly precipitation at Paru Co based on TRMM data from 1998 to 2007 and average monthly temperatures at Paru Co (4845 m asl) from Lhasa (3650 m asl) weather station data using a lapse rate of −6.4 °C km⁻¹ (Huffman et al., 2009). (d) Plot of the age/depth model for Paru Co according to Bird et al. (2014).
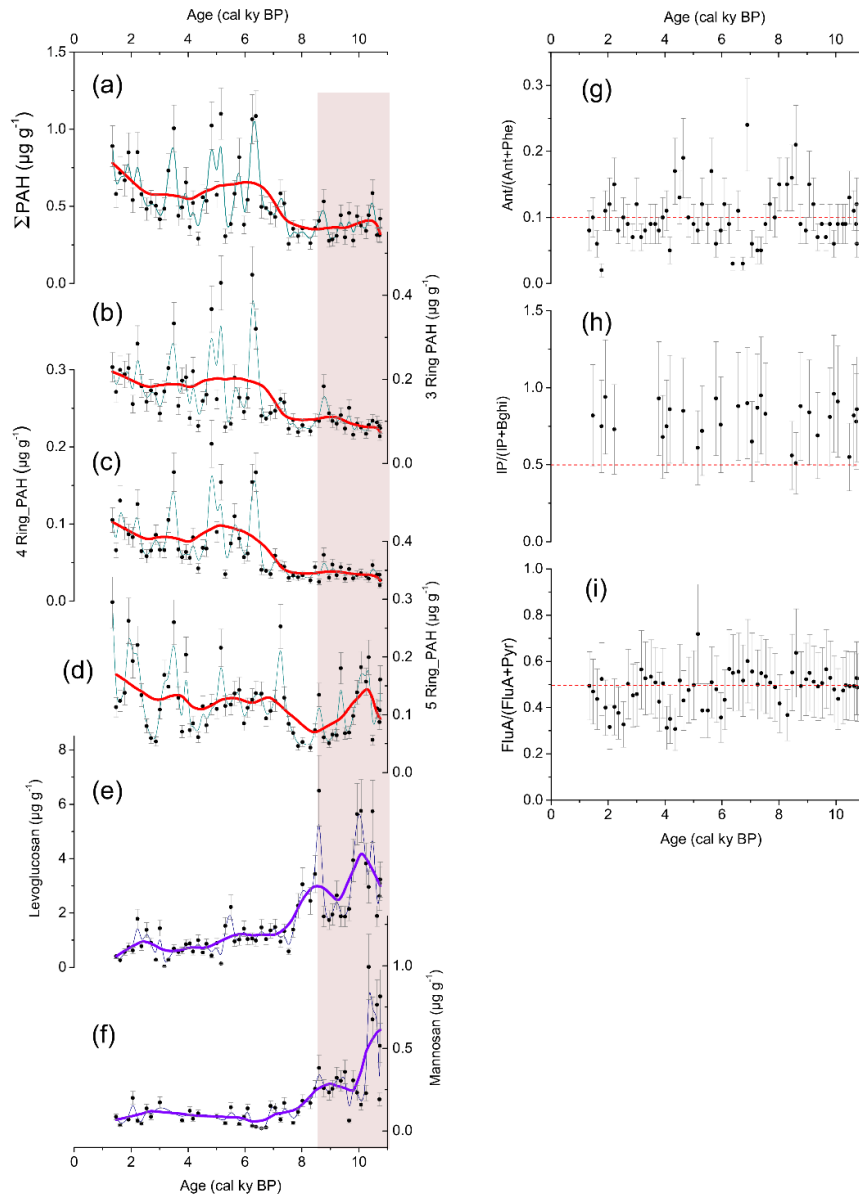
Figure 2: (a) Sum of PAHs concentrations; (b) Sum of 3 ring PAH concentrations (Phe, Ant, FluA); (c) Sum of 4 ring PAH concentrations (Pyr, BaAnt, Chr, Ret, BbFl, Bkfl); (d) Sum of 5-6 ring PAH concentrations (BaPyr, BePyr, Bghi, IP, DBahAnt). Data points (black) with absolute error range (grey), LOWESS smoothing with SPAN parameter 0.2 (red), b-spline interpolation (cyano). (e) Levoglucosan concentration; (f) Mannosan concentration. Data points (black) with absolute error range (grey), LOWESS smoothing with SPAN parameter 0.2 (purple), b-spline interpolation (dark blue). Pink bar indicates the early Holocene period where levoglucosan and 5rings PAHs show high concentrations. (g) Ant/(Ant+Phe); (h) IP/(IP+Bghi); (i) FluA/(FluA+Pyr). Ratios values (black points) with absolute error bars (grey) and diagnostic thresholds (red dashed lines).
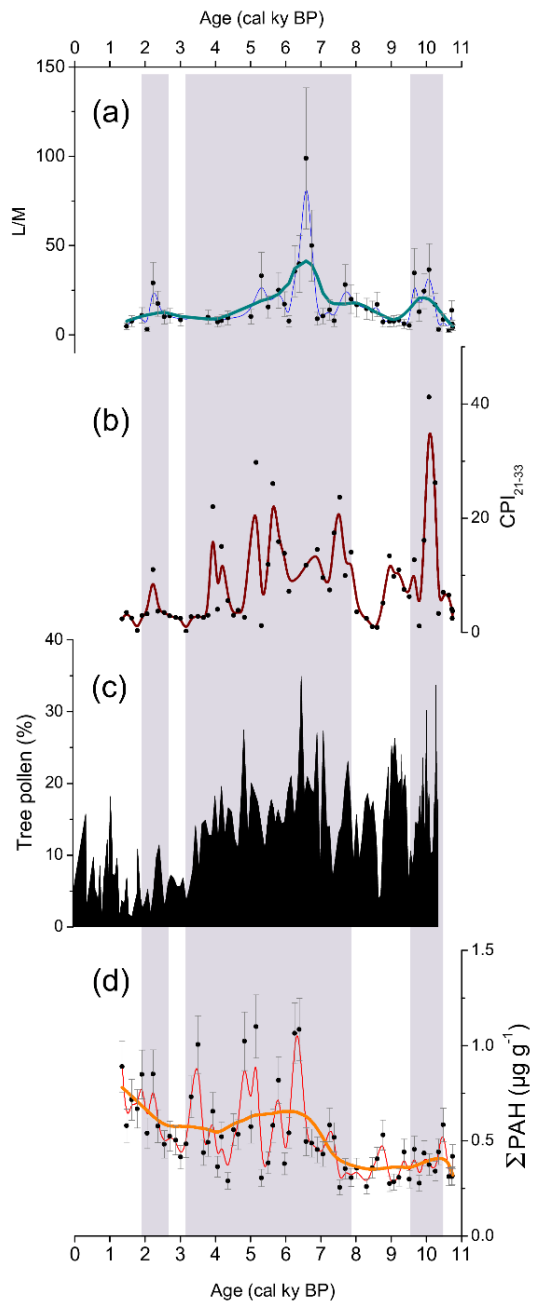
Figure 3: (a) L/M ratio values (black points) with absolute error bars (grey); LOWESS smoothing with SPAN parameter 0.2 (teal), b-spline interpolation (blue). **(b)** CPI ratio values (black points); b-spline interpolation (dark red). **(c)** Tree pollen (%) from Zhao et al., 2011 - http://apps.neotomadb.org/Explorer/?datasetid=14619. **(d)** Sum of PAH concentrations, data points (black) with absolute error range (grey), LOWESS smoothing with SPAN parameter 0.2 (orange), b-spline interpolation (red).
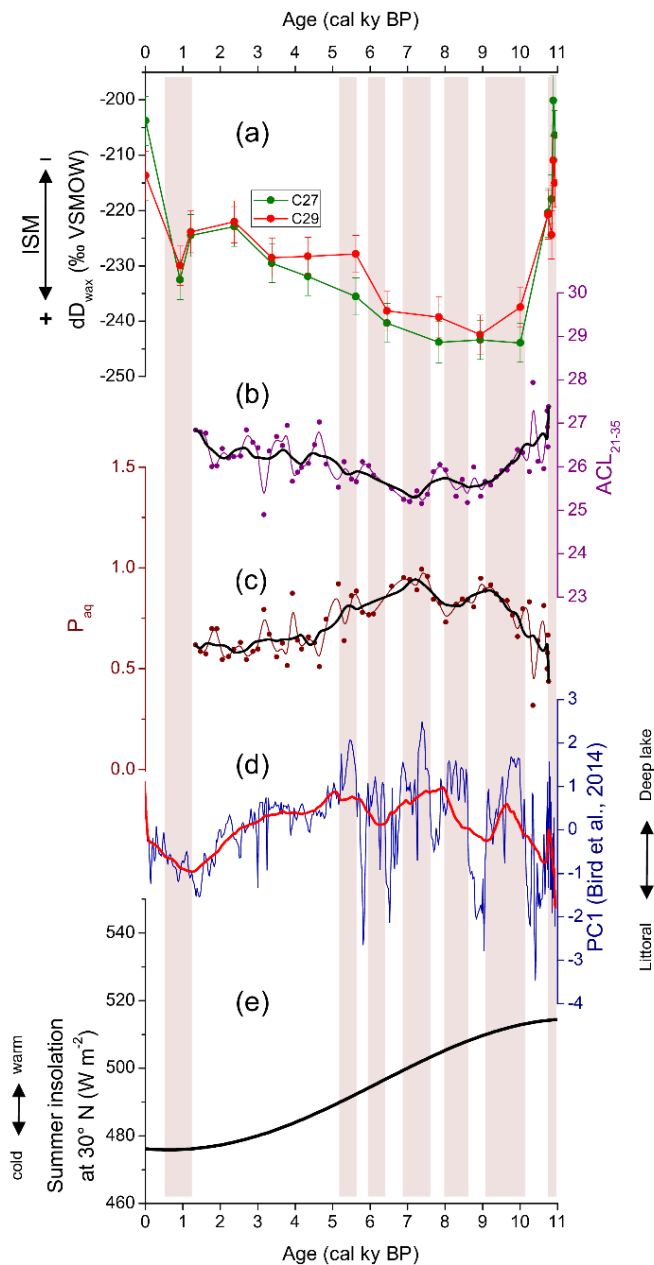
Figure 4: The response of Paru Co aqueous vegetation to changing summer insolation and associated monsoon intensity. (a) δD wax for C27 and C29 n-alkanes referenced to Vienna Standard Mean Ocean Water scale, data from Bird et al., 2014 - https://www.ncdc.noaa.gov/paleo/study/16399. (b) ACL ratio values (purple points), adjacent-average smoothing with 5 points (black), b-spline interpolation (purple line). (c) Paq ratio values (brown points), adjacent-average smoothing with 5 points (black), b-spline interpolation (brown line). (d) Principal component 1 values (blue) as indicative of lake level changes, adjacent-average smoothing with 40 points (red), data from Bird et al., 2014 - https://www.ncdc.noaa.gov/paleo/study/16399 (e) Summer insolation, data from Berger and Loutre (1991).
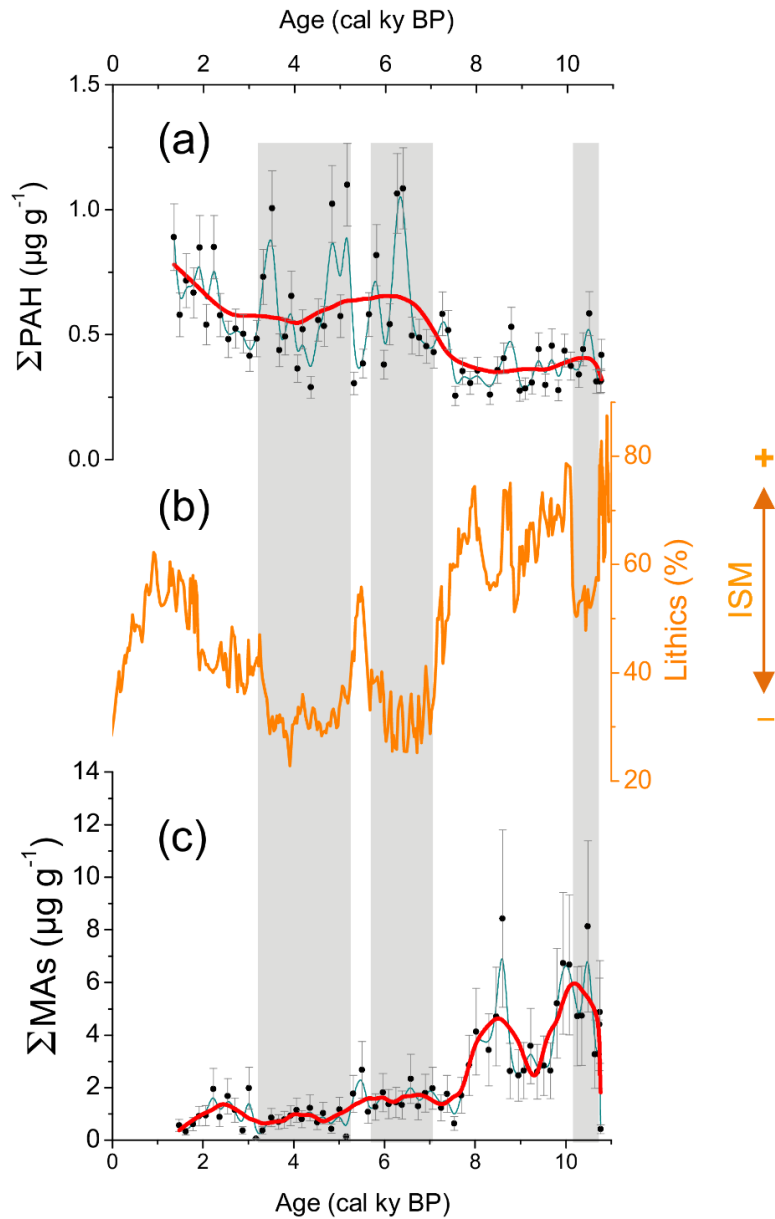
Figure 5: The response of combustion proxies to changes in ISM intensity in Paru Co. (a) Sum of PAHs concentrations, data points (black) with absolute error range (grey), LOWESS smoothing with SPAN parameter 0.2 (red), b-spline interpolation (teal). (b) lithics (%), data from Bird et al. (2014) - https://www.ncdc.noaa.gov/paleo/study/16399. (c) MAs concentrations, data points (black) with absolute error range (grey), LOWESS smoothing with SPAN parameter 0.2 (red), b-spline interpolation (teal).

Table 1: Target molecules with their abbreviations, detected mass to charge ratio (m/z) and method detection limit (ng) calculated as blank values plus three standard deviations or with the signal to noise ratio when no analytes were detectable in the blanks.

Molecular classes	Compounds	Abbreviation	Targeted ion (m/z)	MDL (ng)
MAs	Levoglucosan	L	161	26.1
	Mannosan	M	161	12.2
	Galactosan	G	161	9.8
PAHs	Naphthalene	Naph	128	5
	Acenaphthylene	Acy	152	800 pg
	Acenaphthene	Ace	154	1.2
	Fluorene	Flu	166	3.3
	Phenanthrene	Phe	178	8
	Anthracene	Ant	178	750 pg
	Fluoranthene	FluA	202	2.4
	Pyrene	Pyr	202	2.8
	Benzo(a)anthracene	BaAnt	228	50 pg
	Chrysene	Chr	228	250 pg
	Retene	Ret	219	250 pg
	Benzo(b)fluoranthene	BbFl	252	80 pg
	Benzo(k)fluoranthene	BkFl	252	80 pg
	Benzo(a)pyrene	BaPyr	252	700 pg
	Benzo(e)pyrene	BePyr	252	860 pg
	Benzo(ghi)perylene	Bghi	276	300 pg
	Indeno(1,2,3-c,d)pyrene	IP	276	350 pg
	Dibenzo(a,h)anthracene	DBahAnt	278	800 pg
n-alkanes	C_{10}-C_{35}	C_{10}-C_{35}	71	500
FeSts	Coprostanol	Cop	215	50 pg
	Epicoprostanol	e-Cop	215	50 pg
	Cholesterol	Chl	370	100.4
	Cholestanol	5α-Ch	355	50 pg
	Sitostanol	5α-Sit	215	0.5
	Sitosterol	Sit	215/396	2.3